Chapter 9

# Transition Metal Sulfide Catalysts for Petroleum Upgrading – Hydrodesulfurization Reactions

A. Infantes-Molina, A. Romero-Pérez, D. Eliche-Quesada,
J. Mérida-Robles, A. Jiménez-López and E. Rodríguez- Castellón

Additional information is available at the end of the chapter

http://dx.doi.org/10.5772/45629

## 1. Introduction

Environmental catalysis researchers worldwide have focused much attention on the development of catalytic systems capable of reducing the sulfur amount present in petroleum feedstocks until levels globally established by the recently enacted environmental protection laws. In this regard, the maximum sulfur content present in diesel fuel to obtain an Ultra Low Sulfur Diesel (ULSD) is of 10 ppm in the European Union from the beginning of 2009 with the entry into force of the Euro V fuel standard directive. Meanwhile this limit is slightly higher in the United States, 15 ppm, regulated by the Environmental Protection Agency (EPA) (Hsu & Robinson, 2006). Thus, the development of highly active and selective HDS catalysts, capable of processing these feeds, is one of the most important problems that the petroleum industry has to face nowadays.

Transition metal sulfides (TMS) have been traditionally used as active phases in hydrotreating catalysts since they are known to be efficient systems for catalyzing hydrotreating reactions. Concretely cobalt or nickel promoted molybdenum–tungsten sulfides are well established as the active species for commercial hydrodesulfuration (HDS) catalysts and mainly porous-alumina as a support. Amelioration has been achieved by modifying the properties of these sulfide systems, although the nature of the active phase has hardly been modified during many decades (Song & Ma, 2003). One direction for current research focuses on the use of new types of supports. Studies on nickel sulfided catalysts have concluded that supports, such as $Al_2O_3$, strongly interact with $Ni^{2+}$ ions avoiding their sulfidation (Gil et al., 1994). $Ni^{2+}$-alumina interactions may be weakened by using carriers such as alumina-pillared compounds, where the aluminium oxide is diluted within a layered inorganic matrix inducing a permanent porosity. These materials have been used as catalysts supports in hydrotreating reaction, showing interesting results (Kloprogge

et al., 1993; Occelli & Rennard, 1988). On the other hand, mesoporous silica sieves have become a real alternative to alumina due to their hexagonal array of uniform mesopores and a very high surface area, presenting potential catalytic application for reactions involving bulky molecules, including hydrodesulfurization of petroleum fractions (Corma et al., 1995; Song & Reddy, 1999). In the same way, HMS type materials have been widely studied in this type of reactions (Nava et al., 2011; Zepeda et al., 2005). The intercalation of heteroatoms such as Al, Ti, Ga or Zr into the silica framework not only improves the material stability but also generates new acid, basic or redox functions that extend their application in new fields of catalysis. Thus, zirconium doped mesoporous silica with high surface area, mild acidity and high stability (Rodríguez-Castellón et al., 2003) have shown interesting properties as a support for catalytic fuel processing in reactions such as the hydrogenation, hydrogenolysis and hydrocracking of tetralin (Eliche-Quesada et al., 2003a, 2003b, 2004, 2005). The use of SBA-15 as a support for hydrotreating catalysts has presented several advantages with regard to HMS and MCM-41 mesoporous solids, since SBA-15 material has thicker pore walls and better hydrothermal stability, which are very important properties in hydrotreating processes due to the severe reaction conditions employed (Vradman et al., 2003). Recently, Gómez Cazalilla et al. (Gómez-Cazalilla et al., 2007) have proposed a cheap sol-gel synthesis route for SBA-15 and aluminium doped SBA-15, with sodium silicate as the silica source. The resulting materials have shown interesting properties as catalyst supports in hydrotretating reactions (Gómez-Cazallila et al., 2009a, 2009,b).

Other direction for current research focuses on the use of new active phases for developing high-performance HDS catalysts. The pioneering work of Pecoraro and Chianelli (Pecoraro & Chianelli, 1981) reported the great catalytic activity of bulk transition metals sulfides (TMS). Such metals were plotted into a curve called "volcano plot" where the HDS activity per mole of metal versus the M-S bond strength was plotted, the $RuS_2$ phase being the most active (Toulhoat et al., 1999). Nonetheless when the $RuS_2$ phase is supported, the results found in literature are diverse. On one hand a lower activity was observed due to its reduction into metallic ruthenium under the reducing conditions employed in the catalytic test (De los Reyes, et al., 1990) and if it is supported on alumina, sulfiding temperatures higher than 773 K are required to form the $RuS_2$ phase with pyrite-like structure, which is the true active phase for hydrotreating reactions. Nonetheless, it has been reported that $Ru/\gamma\text{-}Al_2O_3$ catalyst sulfided in 100% $H_2S$ at 673 K possessed about 7-fold higher thiophene conversion rates than $CoMo/\gamma\text{-}Al_2O_3$ when the surface of the active area is considered (Kuo et al., 1988).

Quartararo et al. (Quartararo et al., 2000) perfectly describe that there are many factors during the synthesis of ruthenium sulfide catalysts that must be taken into account for controlling their physicochemical properties, and as a consequence for achieving a good performance with this kind of catalysts. It is recommended no calcination after the incorporation of ruthenium chloride, while the sulfiding mixture should be $H_2S/N_2$ to achieve a high degree of sulfurization and avoid the reduction of the $RuS_2$ phase formed (De los Reyes, 2007). Furthermore, the sulfiding temperature influences the catalytic behaviour (De los Reyes et al., 1991) as well as the crystallographic orientations that induce the

preference toward HDS and hydrogenation (HYD) reactions. One of the main goals to reach is the stabilization of such a phase under the reaction conditions. Ishihara et al. (Ishihara et al., 1992) were the first to report the addition of alkali metals to $RuS_2$ catalysts supported on $Al_2O_3$. The addition of NaOH did not improve the HDS reaction because of the poisoning of some sites. Nonetheless, a cesium-promoted Ru catalyst with Ru/Cs molar ratio of 1:2 exhibited HDS activities comparable to that of conventional Co-Mo catalyst (Ishihara et al., 2003). The insertion of atoms like cesium seems to enhance the number of labile sulfur atoms, aids to stabilize the $RuS_2$ active phase as it strengths Ru-S bond of ruthenium sulfide, promotes the C-S bond scission of dibenzothiophene (DBT) and therefore the catalytic activity increases (Ishihara et al. 2004). However, if a Cs excess is present, the formation of $H_2S$ and regeneration of coordinatively unsaturated sites are prevented, which results in a decrease in the catalytic activity.

With these premises, catalysts for HDS reaction based on molybdenum, tungsten and ruthenium sulfide are described. The role of promoters and material supports on the catalytic activity are reviewed. In this regard, the support effect on HDS activity on molybdenum and tungsten sulfided catalysts promoted with nickel and cobalt are evaluated by using fluorinated alumina $\alpha$-zirconium phosphate materials, zirconium doped mesoporous silica (Zr-MCM) and a commercial $\gamma$-$Al_2O_3$. Moreover the HDS activity of alternative phases such as $RuS_2$ is also described considering not only the role of the support (MCM-41, Zr-MCM-41, $\gamma$-$Al_2O_3$, SBA-15, Zr-SBA-15 and Al-SBA-15) employed but also the addition of a stabilizing agent such as Cs and the cesium precursor salt employed. The catalysts were characterized by X-ray diffraction (XRD), $N_2$ adsorption–desorption isotherms at 77 K, $NH_3$-temperature-programmed desorption ($NH_3$-TPD), X-ray photoelectron spectroscopy (XPS), $H_2$-temperature-programmed reduction ($H_2$-TPRS), transmission electron microscopy (TEM) and DRIFT spectra of adsorbed NO.

## 2. Tungsten and Molybdenum sulfide catalysts

### 2.1. HDS of Thiophene

Nickel, molybdenum and nickel-molybdenum sulfided catalysts supported on alumina-pillared α-zirconium phosphate $Zr[Al_{3.39}O_{1.12}(OH)_{1.60}F_{4.90}]$ $H_{0.57}(PO_4)_2$ (Mérida et al., 1996), with different loadings of Ni and Mo are described. The catalysts were tested in the thiophene HDS reaction at 673 K, using an automatic microcatalytic flow reactor under atmospheric pressure. A hydrogen flow of 50 $cm^3$ $min^{-1}$ containing 4.0 mol% thiophene was fed to the reactor. Monometallic nickel catalysts were prepared following the incipient wetness method with ethyl alcohol solutions of nickel(II) nitrate ($Ni(NO_3)_2$) and nickel metallic loadings of 4, 8 and 12 wt%, denoted as 4wt%Ni, 8wt%Ni and 12wt%Ni, respectively. A catalyst only containing molybdenum (13wt%Mo), was also synthesized with aqueous solution of ammonium molybdate [$(NH_4)_6Mo_7O_{24}{\cdot}4H_2O$]. Finally, another set of catalysts containing both nickel and molibdenum were prepared by successive impregnations with loadings 2.1-9 wt% and 3-13 wt% Ni-Mo. After the impregnation procedure, the catalysts were air dried at 333 K and calcined at 673 K for 5 h. In order to

observe the influence of calcination temperature, 12wt%Ni catalyst was calcined at 623 K and expressed as 12wt%Ni (623 K). The precursors were sulfided at 673 K for 1 h under a flow of 60 $cm^3$ $min^{-1}$ $H_2S/H_2$ (10/90%).

The fluorinated alumina pillared α-zirconium phosphate support ($Al_2O_3$, 29.3 wt%; $S_{BET}$=184 $m^2$ $g^{-1}$) displays a mixed porosity, essentially in the range of mesoporous but with a micropore contribution of ≈ 0.1 $cm^3$ $g^{-1}$, and contain acid sites, mainly of Lewis type, which are active in the dehydration of isopropyl alcohol.

Evidence for formation of metallic sulfides on the support surface was provided by XRD and XPS analyses. XRD analysis revealed the formation of NiS for monometallic nickel sulfide catalysts with a loading higher than 8 wt%, showing very weak diffraction lines, suggesting that this phase should be extremely dispersed and strongly interacting with the support. XRD patterns of Mo and NiMo catalysts only show diffraction peaks corresponding to the $MoS_2$ phase, which are hardly visible, indicating that $Ni^{2+}$ would be inserted into the structure of $MoS_2$ forming a solid solution and for this reason it is not detected.

From XPS measurements, the Ni $2p_{3/2}$ and Mo $3d_{5/2}$ BE values as well as Ni/Zr, Mo/Zr, S/Mo and $S/Ni_{sulf}$ surface atomic ratios for sulfided catalysts are obtained and the corresponding values are included in Table 1. Since the BE of Zr $3d_{5/2}$ and P $2p$ core level electrons were practically constant with values of 183.3 eV and 134.1 eV, respectively, and the P/Zr atomic ratio was maintained close to the theoretical value, P/Zr = 2, it may be inferred that the impregnation-calcination-sulfidation processes did not significantly alter the host framework. The nickel species present on the catalyst surface are nickel(II) sulfide, nickel(II) oxide and $NiAl_2O_4$, as a result of the Ni $2p_{3/2}$ core level spectra decomposition, where three contributions are observed: the first one at 851.3-851.9 eV-NiS; the second one at 854.1 eV-$Ni^{2+}$ in octahedral sites of the supported NiO structure; and a third one at 855.0-855.7 eV-$NiAl_2O_4$ (Okamoto et al., 1977). This means that a fraction of Ni in the oxide form can be sulfided but other fraction remains unsulfided because of its strong interaction with the support that impedes its sulfidation at 673 K. From XPS data, the percentages of $Ni^{2+}$ sulfided are calculated (Table 1). In all cases the percentages of sulfided nickel were lower than 35%, slightly increasing with the metallic content. The $S/Ni_{sulfided}$ surface atomic ratios (Table 1) are close to 1, these values match well with NiS in agreement with XRD data. Regarding the Ni/Zr, it increases with the metallic loading attributed to the higher amount of nickel. The catalyst 12%Ni calcined at lower temperature points to a higher dispersion as from the higher Ni/Zr ratio.

On the other hand, the Ni $2p_{3/2}$ spectra of sulfided NiMo-AlZrP catalysts only show a signal at *ca*. 852.7 eV due to NiS phase indicating that $Ni^{2+}$ is completely sulfided and therefore the environment of this ion in NiMo calcined precursors is different from that of the Ni based materials (851.3-851.9 eV ). A square pyramidal arrangement of $Ni^{2+}$ ions within the $MoS_2$ framework has been proposed (Topsoe et al., 1987) and confirmed by EXAFS spectroscopy (Louwers & Prins, 1992). With regard to Mo $3d$ core level spectra of Mo and NiMo sulfided catalysts, besides the S $2s$ contribution at 226.5 eV (Arteaga et al., 1986), the spectra exhibit the typical Mo $3d_{5/2}$ component at 229.1 ± 0.1 eV characteristic of $MoS_2$ species (Arteaga et

al., 1986). As no significant differences in the BE values are observed, the nature of Mo species may be essentially the same in the catalysts based on Mo and NiMo. The surface Mo/Zr, and Ni/Zr atomic ratios increase with the Mo and Ni contents (Table 1), and are also higher than on monometallic ones indicating a higher dispersion of Mo and Ni on the surface of Ni-Mo catalysts. The surface S/Mo atomic ratios for NiMo catalysts were very close to 2 which are consistent with the formation of $MoS_2$ on the catalysts surface and are higher than that observed on 13%Mo catalyst, indicating higher sulfur content in bimetallic catalysts due to the sulfur bonded to nickel.

| Catalyst Labelling | Binding energy (eV) | | Surface atomic ratios | | | | |
|---|---|---|---|---|---|---|---|
| | Ni $2p_{3/2}$ | Mo $3d_{5/2}$ | Ni/Zr | Mo/Zr | S/Mo | $S/Ni_{sul}$ | $\%Ni_{sul}$ |
| 4%Ni | 855.7-851.8 | | 0.50 | | | 1.06 | 22.6 |
| 8%Ni | 855.6-851.5 | | 0.85 | | | 1.05 | 30.6 |
| 12%Ni | 855.3-851.3 | | 1.01 | | | 1.47 | 34.3 |
| 12%Ni (623K) | 855.4-852.4 | | 1.49 | | | 1.30 | 33.6 |
| 2.1-9%Ni-Mo | 852.7 | 229.1-232.3 | 0.67 | 2.98 | 1.94 | | 100.0 |
| 3-13%Ni-Mo | 852.8 | 229.1-232.3 | 1.16 | 3.82 | 1.98 | | 100.0 |
| 13%Mo | | 229.2-232.3 | | 3.01 | 1.68 | | |

**Table 1.** Binding Energy (BE) and surface atomic ratios as determined by XPS analysis of sulfided catalysts

The catalytic performance of these systems (Ni, Mo and NiMo-AlZrP catalysts) has been evaluated in the thiophene HDS reaction. Thus, from conversion values, the pseudo-first order constant ($k_{HDS}$) was calculated according to the equation:

$$k_{HDS} = -(F/W)\ln(1-x) \tag{1}$$

where, $F$ is the feed rate of thiophene (mol $min^{-1}$), $W$ is the catalyst weight (g) and $x$ is the fractional conversion.

Table 2 compiles $k_{HDS}$ values at the beginning and the end of the reaction (*TOS=6 h*).

As can be seen, Ni-based catalysts show promising $k_{HDS}$ values (between $6{\cdot}10^{-5}$ to $8{\cdot}10^{-5}$ mol $g^{-1}$ $min^{-1}$) without deactivation observed. The catalyst with the highest Ni loading and prepared at lower calcination temperature (623 K) shows the maximum activity with a $k_{HDS}$ value close to $10^{-4}$ mol $g^{-1}$ $min^{-1}$. This activity could be related to both its higher nickel sulfidation and dispersion, as observed from XPS. The sulfided 13%Mo catalyst initially displays a high thiophene HDS activity but undergoes a strong deactivation during the first 0.5 h showing then a similar activity than sulfided Ni catalysts. This behaviour is explained by the presence of coordination vacancies on the edges of $MoS_2$ crystallites. $H_2S$ molecules may occupy these vacancies and act as Brønsted acid sites which provoke the

formation of coke and consequently a drastic decrease of the catalytic activity by blocking the pores and active sites (Yang & Satterfield, 1983). Finally, sulfided NiMo catalysts show a much higher HDS activity than sulfided Ni and Mo ones, which is attributed to both the promoting effect of $Ni^{2+}$ions in the mixed NiMo sulfided materials and the existence of sulfur vacancies (uncoordinated sites) on molybdenum. In this sense, $H_2S$ is not formed directly from the sulfur compound, but from the sulfur on the catalyst surface, being labile that bonded to both Ni and Mo. Thus, $H_2S$ released forms a new vacancy on the catalyst, as reported by Ruette and Ludena (Ruette & Ludena, 1981). These catalysts show high activity for the hydrodesulfurization of thiophene, mainly sulfided NiMo-AlZrP catalysts, which exhibit comparable or even higher activity than Ni, Mo and NiMo sulfided catalysts supported on carbons (Eijsbouts et al., 1994), zeolites (Welters et al., 1994) and alumina pillared smectites (Kloprogge et al., 1993) and tested in similar conditions.

With regards to the selectivity, it is reported in the literature (Silva-Rodrigo et al., 2004) that the reaction of thiophene with $H_2$ over supported HDS catalysts follows two main pathways: (1) direct thiophene hydrogenation leading to tetrahydrothiophene (THT), with further C–S bonding hydrogenolysis to form butane; (2) direct C-S scission to form 1,3-butadiene which is lately hydrogenated to form butene. 1-butene and *cis*- and *trans*-2-butene are intermediary products (Scheme 1). These butane isomers can lately be hydrogenated to form *n*-butane.

| **Catalyst** | **Selectivity (%)** | | | | $k_{HDS}$ **x·10$^5$ (mol g$^{-1}$·min$^{-1}$)** | | $k_{HYD}$**·x 10$^5$ (mol g$^{-1}$·min$^{-1}$)** | $k_{HYD}/k_{HDS}$ |
|---|---|---|---|---|---|---|---|---|
| | n-b | 1-b | 2-t-b | 2-c-b | Initial | *TOS* 6h | | |
| 4%Ni | - | 27.5 | 35.0 | 37.5 | 7.50 | 6.22 | - | - |
| 8%Ni | - | 28.0 | 36.0 | 36.0 | 9.24 | 8.16 | - | - |
| 12%Ni | - | 29.0 | 35.0 | 36.0 | 7.75 | 7.15 | - | - |
| 12%Ni (623K) | - | - | - | - | 11.39 | 8.42 | - | - |
| 2.1-9%Ni-Mo | 17.5 | 25.0 | 27.0 | 30.5 | 48.53 | 16.01 | 4.68 | 0.30 |
| 3-13%Ni-Mo | 12.0 | 18.0 | 35.0 | 35.0 | 60.37 | 21.23 | 4.34 | 0.20 |
| 13%Mo | 12.0 | 21.0 | 33.0 | 34.0 | 22.50 | 6.07 | 7.80 | 1.28 |

n-b: n-butane; 1-b: 1-butene; 2-t-b: 2-t-butene, 2-c-b: 2-c-butene

**Table 2.** Pseudo-first-order rate constants for HDS of thiophene and selectivity values to different reaction products after 6 hours on stream

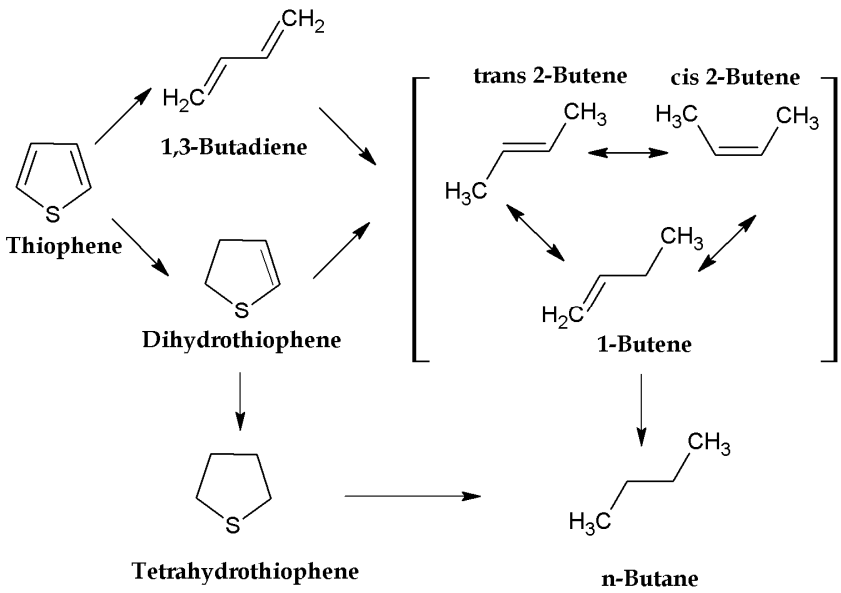


**Scheme 1.** Reaction scheme of HDS of Thiophene over Ni and NiMo sulfided catalysts

The reaction products identified by gas chromatograph where *n*-butane, 1-butene and *cis* and *trans*-butene (Table 2). It is noticeable different selectivities for these catalysts, thus monometallic Ni ones do not produce the hydrogenation product, butane. The hydrogenation ability of the catalyst can be interpreted by the presence of active hydrogen generated on molybdenum sites. Hydrogen activation takes place through intercalation in $MoS_2$ by proton permeation in the van der Waals gap and by stabilizing the electron charge in the 2*p*-band of sulfur. From $k_{HYD}/k_{HDS}$ ratios, summarized in Table 2, 13%Mo catalyst possesses the highest value confirming that it is molybdenum the responsible for the hydrogenation capability of these catalysts.

Characterization results indicated that the total sulfidation of $Ni^{2+}$ ions only occurred in NiMo catalysts, where a higher dispersion of the active species was also observed. These factors explain the high activity observed in thiophene HDS reaction, assigned to the promoter effect of Ni, which in turns diminishes the hydrogenation capability of the catalyst. NiMo catalyst with the highest metallic loading, 3-13%Ni-Mo, showed the maximum activity, $k_{HDS}$=21.2 $10^{-5}$ mol $g^{-1}$ $min^{-1}$. All the catalysts presented a similar behaviour, i.e., after an initial deactivation period, the catalyst maintained its activity for a long time attributed to the presence of Lewis acid sites in the support that avoids the formation of coke. Moreover, after reaction, no sulfur loss was detected by XPS analysis (data not shown), with BE values of Ni and Mo being in the range of the sulfided forms, pointing to the high stability of these catalysts under the conditions employed. These results show the interesting properties of alumina pillared α-zirconium phosphate to be used as hydrotreating support.

## 2.2. HDS of Dibenzothiophene (DBT)

The properties of Ni-Mo(W) and Co-Mo(W) catalysts supported on zirconium doped MCM-41 (Zr-MCM) are described and their activity in the HDS reaction of DBT compared with a catalyst supported on commercial $\gamma$-$Al_2O_3$. The HDS of DBT was carried out at 3.0 MPa of total pressure, $H_2$ flow rate of 100 $cm^3$ $min^{-1}$ and weight hourly space velocities (WHSV) of 32 $h^{-1}$. Thus Ni-W, Ni-Mo, Co-W and Co-Mo catalysts (W = 20 wt%; Mo= 11 wt%; Ni and Co = 5 wt%) were prepared by the incipient wetness method using mixed solutions of ammonium metatungstate (Aldrich) and nickel(II) citrate or cobalt(II) nitrate (Aldrich) in the case of Ni(Co)-W catalysts, or a mixed solution of ammonium heptamolybdate (Aldrich) and nickel(II) citrate or cobalt(II) nitrate for Ni(Co)-Mo catalysts. All materials, after impregnation with the metallic salts, were dried and calcined at 823 K for 4 h. These calcined precursors were then sulfided at 673 K with a $N_2/H_2S$ (90/10%) flow of 60 $cm^3$ $min^{-1}$ for 2 h prior to the catalytic test. The catalysts are labelled as Ni(Co)(*x*)-Mo(W)(*y*), where *x* denotes nickel or cobalt content (wt%); and *y*, molybdenum or tungsten content (wt%).

The support chosen in this study is zirconium doped mesoporous silica (Zr-MCM) that possesses a hexagonal array of mesoporous pores (30 Å), very high surface area ($S_{BET}$= 608 $m^2$ $g^{-1}$) and an induced acidity (mild strength) due to the incorporation of zirconium into the mesoporous structure that also provides higher stability (Rodríguez-Castellón et al., 2003). After impregnation-calcination-sulfidation, the mesoporous structure is not altered as observed from XRD and $N_2$-adsorption-desorption isotherms.

Characterization results of sulfided catalyst by XRD indicate that tungsten promoted catalysts (Ni(Co)5-W20) showed not well defined diffraction peaks, pointing to a low crystalline $WS_2$ phase; while molybdenum based catalysts (Ni(Co)5-Mo11) presented well defined diffraction peaks corresponding to the $MoS_2$ phase. In general, nickel promoted catalysts present a better dispersion of Mo or W species as the lower intensity of $MoS_2$ and $WS_2$ diffraction peaks on these catalysts indicates. In no case, diffraction lines of nickel or cobalt sulfide are observed, suggesting that these phases are very dispersed or inserted into $WS_2$ or $MoS_2$ structure, forming a well dispersed Ni(Co)-W(Mo)-S solid solution, as it was observed before. The textural parameters of the support and the different sulfided catalysts (Table 3) reflect an important reduction of the specific surface area and pore volume after the incorporation of the active phase. This decrease could be attributed not only to the presence of particles of Ni(Co)-W(Mo)-S partially blocking the mesopores, but also to the increase in the density of the materials after the incorporation of a Ni(Co)-W(Mo)-S species.

The chemical species present on the surface of sulfided samples and their relative proportions were evaluated by XPS. The corresponding spectral parameters are included in Table 3. All sulfided catalysts present a maximum at 161.9 eV in the S 2*p* energy region, which is characteristic of sulfide ($S^{2-}$) species. The W 4*f* core level spectra indicate the presence of mainly tungsten sulfide $WS_2$ (32.4 eV) and non-sulfided W(VI) species or partially sulfided O-W-S species (36.2 eV) (Benítez et al.,1996). Mo 3*d* core level spectra exhibit the typical Mo $3d_{5/2}$ component characteristic of $MoS_2$ species at 228.5 eV and a weak contribution at higher B.E. (229.8 eV) due to partially sulfided O-Mo-S (Pawelec et al., 2003).

For Ni promoted catalysts, the Ni $2p_{3/2}$ photoemission line presents contributions at ca. 853.6 eV (nickel sulfide) and 856.5 eV ($NiWO_4$). The high BE for $Ni^{2+}$ forming a sulfide phase also suggests that $Ni^{2+}$ ions are embedded in the structure of $WS_2$ or $MoS_2$, probably forming the Ni-W(Mo)-S phase. Similarly, the Co promoted catalysts showed evidence for cobalt mainly in a sulfide phase (778.5 eV) (Alstrup et al., 1982) and a minor one at 781.3 eV, due to tetrahedral Co in an oxidic environment (Infantes-Molina et al., 2005).

| Sample | $S_{BET}$ ($m^2g^{-1}$)[a] | $V_p$ ($cm^3g^{-1}$)[a] | $d_p$(av) (Å)[a] | Binding Energy (eV)[b] | | | |
|---|---|---|---|---|---|---|---|
| **Zr-MCM** | 608 | 0.49 | 29.9 | **Ni $2p_{3/2}$** | **Co $2p_{3/2}$** | **W $4f_{7/2}$** | **Mo $3d_{5/2}$** |
| **Ni5W20** | 332 | 0.25 | 24.1 | 853.6<br>856.4 | | 32.4<br>36.2 | |
| **Co5W20** | 276 | 0.23 | 27.2 | - | 778.5<br>781.3 | 32.4<br>36.3 | |
| **Ni5Mo11** | 271 | 0.21 | 25.9 | 853.6<br>856.4 | - | | 228.5<br>229.7 |
| **Co5Mo11** | 241 | 0.21 | 29.2 | | 778.4<br>781.3 | | 228.4<br>229.9 |

**Table 3.** Textural properties[a] from $N_2$ adsorption-desorption isotherms at 77 K and spectral parameters[b] obtained by XPS analysis of sulfided catalysts

The dispersion of active phases on the sulfided catalysts was estimated from the surface atomic ratios. Table 4 compiles the Ni(Co)/(Si+Zr), Mo(W)/(Si+Zr) and S/Mo(W) atomic ratios. Ni/(Si+Zr) and Co/(Si+Zr) ratios are higher for molybdenum catalysts, showing a higher dispersion of the promoters on these catalysts (Ni(Co)-Mo). With regards to Mo(W)/(Si+Zr) atomic ratios, these are higher for nickel promoted catalysts, indicating a better superficial dispersion of these phases under the presence of nickel. The S/W atomic ratios for Ni(Co)-W catalysts are very close to 2, which is consistent with the formation of $WS_2$ on the catalyst surface, and it is also higher for nickel promoted catalyst (Ni5-W20). Meanwhile S/Mo ratios are much more high for both catalysts, being greater for Ni5-Mo11 one. These data suggest the higher degree of sulfidation for molybdenum based catalysts, as deduced from the TPRS data (*vide infra*) and also when nickel is present that also facilitates the dispersion of W and Mo.

| | Surface atomic ratios | | | | | |
|---|---|---|---|---|---|---|
| **Sample** | **Ni/X** | **Co/X** | **W/X** | **Mo/X** | **S/W** | **S/Mo** |
| **Ni5-W20** | 0.115 | - | 0.110 | - | 2.53 | - |
| **Co5-W20** | - | 0.089 | 0.096 | - | 1.85 | |
| **Ni5-Mo11** | 0.196 | - | - | 0.090 | - | 5.43 |
| **Co5-Mo11** | - | 0.119 | - | 0.037 | - | 4.04 |

**Table 4.** Surface atomic ratio of sulfided catalysts obtained by XPS analysis. X = Si + Zr

The nature of sulfur species as well as their stability is determined by $H_2$-TPRS measurements. From these experiments it is concluded that nickel promoted catalysts present a higher amount of $H_2S$ released at ca. 543 K. This removal of $H_2S$ comes from nickel or cobalt sulfide located at the edges of $WS_2$ or $MoS_2$ slabs forming the Ni(Co)-W(Mo)-S active phase (Magnus & Moulijn, 1994) and ascribed to the formation of coordinatively unsaturated sites (CUS) on the edge planes of the Ni(Co)-W(Mo)-S phase, being the active sites in HDS reaction. Therefore, nickel catalysts present a higher amount of active sites (CUS sites) on these catalysts. This also may explain the higher HDS activity observed for Ni5-W20 and Ni5-Mo11 catalysts (*vide infra*). Moreover, the curves are more intense for Mo catalysts, indicating a higher sulfurization degree when molybdenum is present, as obtained from XPS (*vide supra*).

The activity of these catalysts was evaluated in the DBT HDS model reaction. For DBT HDS, it has been proposed (Bataille et al., 2000) that the reaction proceeds through the hydrogenolysis pathway, the direct desulfurization route (DDS), leading to the production of biphenyl (BP); or by a second hydrogenation reaction pathway (HYD), in which one of the aromatic rings of dibenzothiophene is firstly prehydrogenated, forming tetrahydro (THDBT)- and hexahydro-dibenzothiophene (HHDBT), which is later desulfurized to form cyclohexylbenzene (CHB) (Scheme 2).

From conversion values and by applying equation (1), pseudo first order constants ($k_{HDS}$) were determined for HDS of DBT. The corresponding values are plotted in Figure 1.A, where it is observed that the activity increases with the temperature. At high reaction temperatures the activity follows the order: Ni5-Mo11> Ni5-W20> Co5-Mo11> Co5-W20, being always Ni-based catalysts much more active than their counterparts with cobalt. This fact could be related to the higher sulfidation degree and dispersion of nickel containing catalysts as observed in XPS and XRD, and the greater presence of CUS sites as observed from TPRS studies.

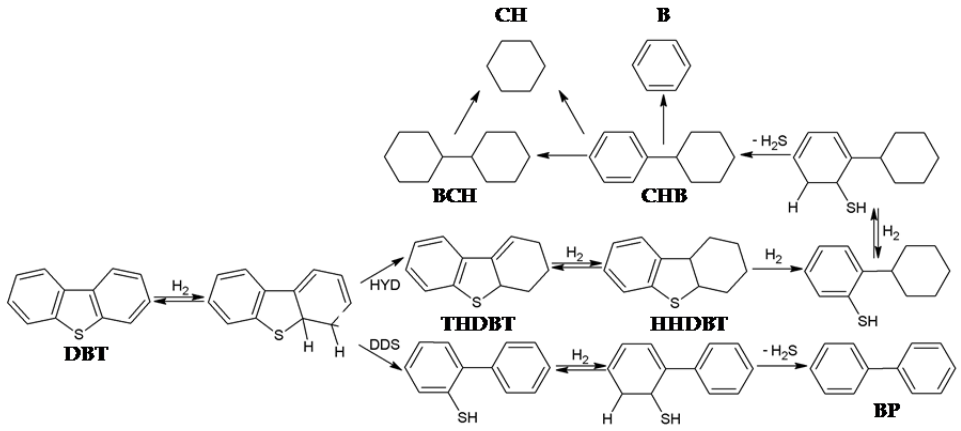


**Scheme 2.** Reaction scheme of HDS of DBT over Ni(Co)Mo(W) sulfided catalysts: HYD: hydrogenation route; DDS: direct desulfurization route; DBT: dibenzothiophene; BP: biphenyl; THDBT: tetrahydrodibenzothiophene; HHDBT: hexahydrodibenzothiophene; CHB: cyclohexylbenzene; BCH: Bicyclohexyl; CH: Cyclohexane; B: Benzene.

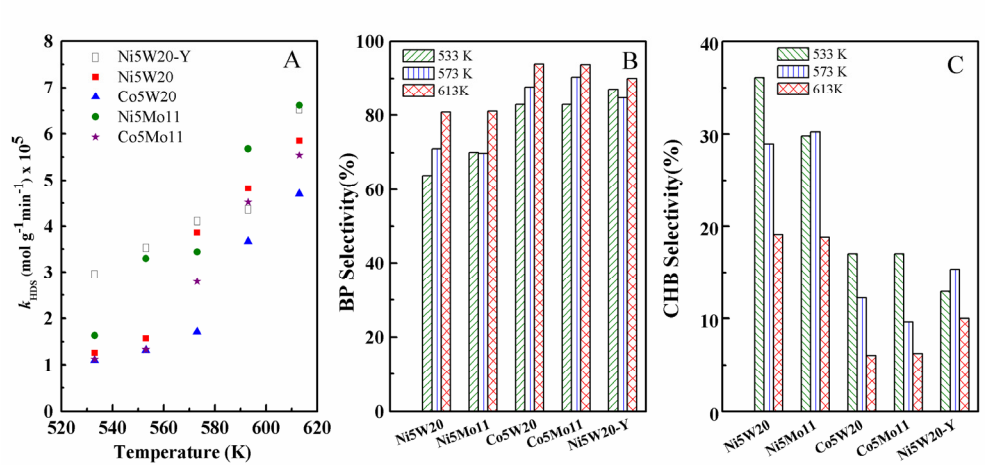


**Figure 1.** Influence of reaction temperature on HDS activity. Reaction conditions T= 533-613 K; P=30 bar, WHSV=32 $h^{-1}$, $H_2$= 100 $cm^3$ $min^{-1}$

The observed activity in the DBT HDS reaction with this set of catalysts is better than those reported for other catalysts prepared by using MCM-41 as support, such as CoMo (Song & Reddy, 1999), NiMo (Grzechowiak et al., 2006) and NiMo and CoMo supported on non proton-exchanged MCM-41 (Li et al., 2003). Moreover, the comparison with a catalyst supported on a commercial support such as $Al_2O_3$ (BET surface area: 302 $m^2$ $g^{-1}$ and pore volume: 0.33 $cm^3$ $g^{-1}$), denoted as Ni5W20-Y, shows that in spite of the higher activity at lower temperatures, at higher temperatures Ni5Mo11 and Ni5W20 catalysts reach and overcome the activity reported by the Ni5W20-Y catalyst.

With regards to the selectivity shown by these catalysts, Figure 1 also plots the selectivity to the direct desulfurization product (DDS), biphenyl (BP) (Figure 1.B); and to the hydrogenation (HYD) product, cyclohexylbencene (CHB) (Figure 1.C), of the sulfided catalysts as a function of reaction temperature. It is noticeable that the product distribution markedly changes with the promoter, since the formation of the hydrogenation product, CHB, is higher for both nickel promoted catalysts. The formation of CHB increases at the expense of BP. So, whatever the active phase may be (Mo, W), the presence of Ni as a promoter leads to a considerable increase in the HYD reaction. Further, and in agreement with the thermodynamic restrictions, given that the hydrogenation reaction is exothermic, a decrease in hydrogenation activity is observed with an increase in the reaction temperature for all catalysts (Farag et al., 2000). It is generally accepted that hydrogenation and desulfurization reactions take place on separate active sites (Li et al., 2002). It is assumed that the enhancement of the HYD pathway is attributed to the strong hydrogenation properties of the Ni species, and it is proposed that hydrogenation occurs on other sites (such as Ni atoms), while the removal of the sulfur atom from the dibenzothiophene ring takes place on the Ni-Mo(W) cluster. These results are in accordance with findings by Wang et al. (Wang et al., 2002), who compared the CHB/BP selectivity ratio for a series of Ni, Mo

and Ni-Mo sulfided catalysts supported on MCM-41 and established that all the Ni-Mo/MCM-41 catalysts yield a higher ratio than single Mo or Ni/MCM-41, suggesting that there is a synergetic effect between Ni and Mo sulfides in the HYD pathway during HDS. In fact, according to Whiterhurst (Whiterhurst et al., 1998), the rate constant of HDS after hydrogenation of one aromatic ring of DBT is 33 times greater than that of DDS for this kind of catalyst. The enhanced hydrogenation capability of these catalysts has been previously observed, since Ni-W sulfides supported over Zr-MCM-41 exhibit up to 44% conversion in the hydrogenation of tetralin to decalins (Eliche-Quesada et al., 2003b).

The hydrogenation properties observed for these catalysts can also be ascribed to the presence of superficial zirconium species on the surface of Zr-MCM that along with its high surface area, seem to have an influence on the dispersion and specific electronic properties of the active species. In this sense, it is proposed that the presence of smaller slabs increases the number of rim sites which are responsible for hydrogenation reaction, according to the rim-edge model for HDS reaction (Whiterhurst et al., 1998). Our results are in agreement since the catalysts showing higher hydrogenating properties, Ni promoted catalysts, present better dispersion of Ni, Mo and W as extracted from XRD and XPS. The results are quite interesting since nickel promoted catalysts (Ni-Mo(W)) supported on Zr-MCM not only present high HDS activity but also a better hydrogenation capability leading to a gas-oil with improved quality such as higher cetane number.

By contrast, HDS over Co promoted catalysts supported on Zr-MCM, Co-Mo(W) sulfided catalysts, mainly follow the route of hydrogenolysis. The introduction of Co to Mo(W)-based catalysts enhances the direct extraction of sulfur atoms from the DBT molecules. It is assumed that Co sulfide acts by extracting sulfur atoms directly from the sulfur-containing molecules. This is essentially due to the low rate of HYD of Co-Mo(W) sulfides. In conclusion, with Ni promoted catalysts (Ni-Mo(W)), the HYD pathway is dominant over the hydrogenolysis pathway in the HDS reaction of DBT, whereas the direct DDS of DBT occurs with Co-Mo(W) catalysts. The comparison with the commercial catalyst reveals that the selectivities to hydrogenation product (CHB) are higher for the Zr-MCM-derivative (Figure 1), being the selectivity to Ni5W20-$Al_2O_3$ only a half of that found for its Zr-MCM counterpart, possibly due to the higher particle size formed over $Al_2O_3$.

## 3. Ruthenium sulfide catalysts

Supported ruthenium sulfide catalysts were studied in the hydrodesulfuration (HDS) of dibenzothiophene (DBT). The role of the support, sulfiding temperature, the presence of Cs as $RuS_2$-stabilyizing agent, as well as the ruthenium precursor salt employed was studied. Ruthenium was incorporated by the incipient wetness impregnation procedure adding an aqueous solution of ruthenium(III) chloride ($RuCl_3 \cdot nH_2O$) to the pelletized support (0.85-1.00 mm) to obtain catalysts with 7 wt% of ruthenium. After air-dried, the samples were directly sulfided in situ at atmospheric pressure with a $N_2/H_2S$ (90/10%) flow of 60 $cm^{-3}$ $min^{-1}$ by heating from rt. to the sulfidation temperature (Ts) (2 h) at a heating rate of 10 K $min^{-1}$.

### 3.1. Influence of the material support

The supports employed were MCM-41 mesoporous silica (Rodríguez-Castellón et al., 2003); that doped with zirconium (Zr-MCM) (Rodríguez-Castellón et al., 2003); SBA-15 mesoporous silica (Gómez-Cazalilla et al., 2007); SBA doped with zirconium (Zr-SBA) and aluminium (Al-SBA) (Gómez-Cazalilla et al., 2007). Finally a commercial $\gamma$-$Al_2O_3$ was also employed as reference. The supports, precursor, sulfided and spent catalysts were characterized by a variety of experimental techniques in order to establish a clear catalyst performance-structure correlation.

The prepared catalysts are sulfided at 673 K and their catalytic activity evaluated in the HDS of DBT between 533 K and 613 K. The $k_{HDS}$ values (Eq. 1) versus reaction temperature are plotted in Figure 2. In all cases there is a direct improvement in the activity as a function of the reaction temperature. At low temperature, RuSiSBA and RuZrMCM are the most active catalysts, although all of them present $k_{HDS}$ values lower than $0.5.10^{-5}$ mol $g^{-1}$ $min^{-1}$. The influence of the support becomes more evident at higher temperature, where SBA-15 type supports provides more active catalysts than MCM-41 ones, with pure silica supported catalyst, RuSiSBA, the most active at 613 K. The catalyst prepared with a commercial support is the least active catalyst. The results presented here highlight the importance of the usage of mesoporous materials as supports, which could be probably ascribed to the better dispersion achieved on these materials.

By considering the selectivity data (Scheme 2), all the catalysts preferentially follow the DDS route, i.e., the formation of biphenyl is favoured in all cases (Figure 2). The influence of the reaction temperature reveals that its formation slightly increases with the temperature, due to thermodynamics considerations. The formation of the product coming from the HYD route, cyclohexylbenzene (CHB) decreases with the increase of the temperature (Figure 2), being the catalysts supported on Al-SBA-15 type materials, the least selective to this compound, and that supported on the commercial support, Ru-$Al_2O_3$, the catalyst with the best hydrogenating properties.

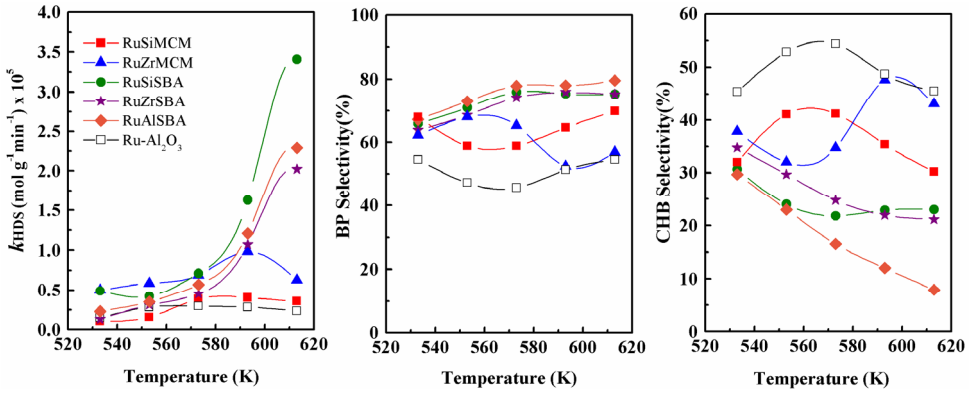


**Figure 2.** Influence of the support on the $RuS_2$ DBT HDS activity and selectivity as a function of reaction temperature. Experimental conditions: P=30 bar, WHSV=32 $h^{-1}$ and $H_2$ flow=100 $cm^3$ $min^{-1}$.

It can be clearly seen that the presence of heteroatoms into the silica mesoporous structure affects the catalytic response of the catalyst. Thus, the presence of zirconium in MCM-41, improves the HDS activity with regards to the catalyst supported on pure MCM-41 (RuZrMCM versus RuSiMCM), and also alters the selectivity, with a greater selectivity to CHB at higher temperatures. Nonetheless, an opposite trend is observed on SBA-based catalysts, since RuSiSBA presents the highest activity values, while the incorporation of aluminium (post-synthesis) and zirconium (direct synthesis) do not provoke any amelioration, only a slight increase in the formation of hydrogenation product is observed at lower temperatures for RuZrSBA. All these data points to a different Si and Zr environment in both mesoporous supports that has a strong influence on the $RuS_2$ phase formed after sulfidation. In this regard, the incorporation of zirconium into MCM-41 has a positive effect, since it could act as $RuS_2$ stabiliser avoiding its reduction under the experimental conditions employed, as well as incorporating acidic functions to the catalyst that could enhance the DBT HDS reaction. Nonetheless, when using SBA-15, in spite of increasing the acidity of the material, a depletion of catalytic activity is observed and therefore suggesting that it is not the acidity but other factors those governing the catalytic behaviour of these systems.

From catalytic data previously exposed, it is observed that $RuS_2$ phase on SBA-15 type support is more active for S-removal and that is why the influence of the sulfiding temperature has been evaluated on these systems, by comparing the HDS activity after sulfidation at 673 K and 773 K. The corresponding results are compiled in Figure 3. From this figure, the catalysts sulfided at 673 K are less active at all studied temperatures. Regarding catalysts sulfided at 773 K, those supported on Si-SBA and Zr-SBA present a similar behaviour with RuAlSBA catalyst the least active. This catalyst only shows a slight improvement at moderate temperatures after sulfiding at 773 K. With regards to the selectivity trend (data not shown here) it is only observed a slight increase of the HYD route by increasing the sulfidation temperature for RuSiSBA and RuZrSBA, what should be related to the formation of more active phase, while RuAlSBA is the most selective to BP at all studied reaction and sulfidation temperatures.

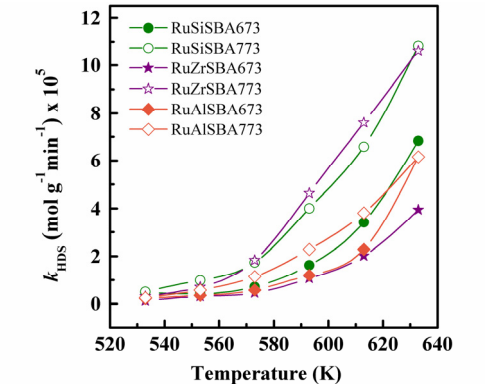


**Figure 3.** Influence of the sulfidation temperature on the catalytic behaviour of $RuS_2$ supported on SBA-15 type materials.

In order to find a possible explanation of catalytic results, catalysts characterization was performed. In this regard, XRD patterns of sulfided catalysts at 673 K supported on MCM-41 and γ-$Al_2O_3$ did not show the characteristic diffraction peaks of $RuS_2$, while XRD patterns of catalysts supported on SBA-15 presented such peaks at 2θ=31.8º, 45.7º and 54.2º (PDF Card Nº. 00-012-0737) at both sulfidation temperatures as observed in Figure 4.

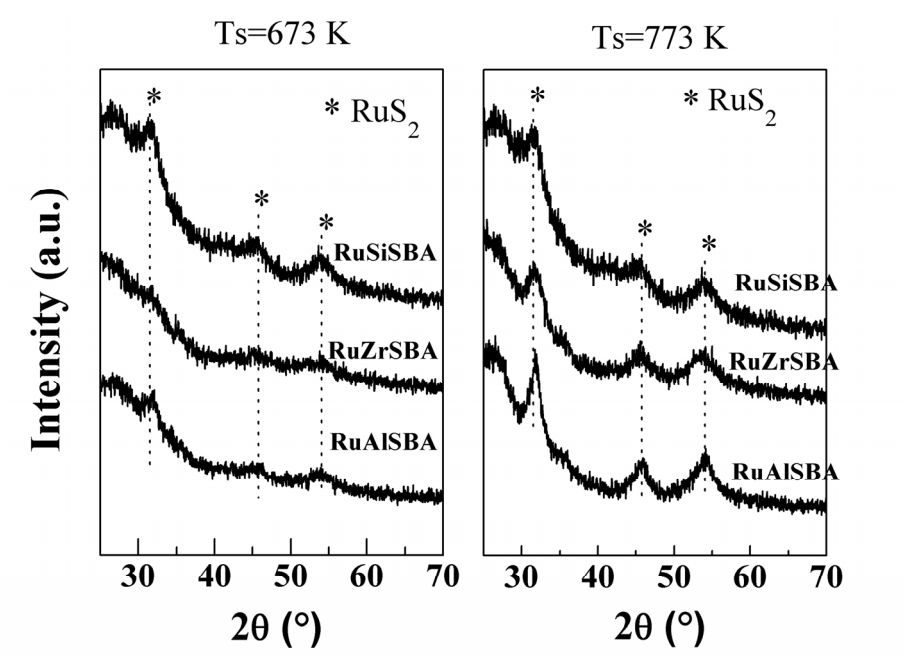


**Figure 4.** XRD patterns of SBA supported catalysts sulfided at 673 K and 773 K.

From this figure it is noticed that by sulfiding at 673 K, a poorly crystalline ruthenium sulfide phase is formed that undergoes reduction under hydrogen hydrotreating atmosphere, as seen from XRD of spent catalyst (data not shown). Therefore a sulfidation temperature of 673 K seems to be insufficient to form stable $RuS_2$ particles. Possibly particles with a stoichiometry of $RuS_{2-x}$ have been formed. These data are in agreement with the catalytic results, where the less active catalysts, RuSiMCM, RuZrMCM, Ru-$Al_2O_3$, do not show these peaks; while RuSiSBA presenting these lines better defined is the most active one. On the contrary, the catalysts sulfided at 773 K do not present the diffraction signals of metallic ruthenium after the catalytic run. Therefore, at 773 K, a greater proportion of the pyrite phase is formed, which is highly stable under reaction conditions. The presence of heteroatoms into the mesoporous structure provokes a greater interaction with the precursor and higher sulfidation temperatures are required as can be clearly seen from XRD patterns of RuZrSBA, presenting so a lower catalytic activity with regards to pure SBA.

The textural and acidic properties of the catalysts are compiled in Table 5.

| Sample | $S_{BET}$ ($m^2\ g^{-1}$)[a] | $V_p$ ($cm^3\ g^{-1}$)[a] | $d_p$ (nm)[a] | μmol $NH_3 \cdot g^{-1}$ [b] |
|---|---|---|---|---|
| SiMCM | 784 | 0.54 | 2.3 | 127 |
| RuSiMCM | 731 | 0.48 | 2.2 | 139 |
| ZrMCM | 608 | 0.49 | 3.0 | 474 |
| RuZrMCM | 501 | 0.40 | 2.6 | 504 |
| $Al_2O_3$ | 313 | 0.44 | 4.8 | 731 |
| Ru- $Al_2O_3$ | 280 | 0.35 | 3.9 | 780 |
| Si-SBA | 476 | 0.35 | 3.9 | 144 |
| RuSiSBA673 | 331 | 0.25 | 3.5 | 272 |
| Zr-SBA | 495 | 0.40 | 3.7 | 1081 |
| RuZrSBA673 | 327 | 0.26 | 3.7 | 798 |
| Al-SBA | 360 | 0.29 | 3.7 | 192 |
| RuAlSBA673 | 222 | 0.18 | 3.2 | 469 |

**Table 5.** Textural[a] and acidic properties[b] of supports and catalysts sulfided at 673 K

These data indicate that catalysts supported on MCM-41 present a much higher surface area and pore volume than those supported on SBA-15, although a much lower pore diameter; while the acidity values do not follow any trend. In all cases, an increase in the acidity is observed after the incorporation of $RuS_2$. It has been reported that the acidity of ruthenium sulfided catalysts is due to the presence of different species on the surface: coordinatively unsaturated sites (CUS) that provide Lewis acidity as well as $SH^-$ groups providing Brønsted acidity (Berhault et al., 1998). It cannot be established a clear correlation between textural/acidity properties and catalytic activity, although the higher pore diameter of SBA type support could favor a better distribution of the active phase inside the channels.

Information regarding the different sulfur species present on the catalyst, the degree of sulfidation attained as well as the stability of the active phase, can be obtained from $H_2$-TPRS profiles. Thus, the $H_2$-TPRS patterns of sulfided ruthenium catalysts are shown in Figure 5, where $H_2S$ removal signals are depicted as a function of temperature. De los Reyes et al. (De los Reyes et al., 1991) have pointed that the reduction of ruthenium sulfide based catalysts takes place in several steps. The first $H_2S$ removal at low temperatures ($T < 450$ K) is due to the surface sulfur excess which is formed during the sulfidation due to the lack of hydrogen, and/or could also be due to sulfur coordinated to surface Ru. In the second $H_2S$ removal, between 450 K and 570 K, the elimination of surface sulfur anions occurs. Some authors have found that this band tends to disappear by sulfiding at higher temperatures, suggesting that this band arises from the reduction of an amorphous or poorly crystallize $RuS_2$ phase at low sulfiding temperatures (Castillo-Villalón et al., 2008) and also ascribed to the release of labile sulfur (CUS). Finally, at $T > 573$ K, the elimination of bulk sulfur of the $RuS_2$-pyrite takes place leading to metallic ruthenium (Castillo-Villalón et al., 2008; De los Reyes et al., 1991).

Catalysts supported on MCM-41 type support possess a similar $H_2S$ desorption profile, with the exception of the temperature peak at lower temperatures, that is hardly observed for RuSiMCM and a higher intensity of the second desorption peak for RuZrMCM assigned to the presence of CUS sites. The catalytic activity of these two samples is different. These results point to the presence of zirconium as responsible for such a fact. The presence of zirconium has a manifold role; it could lead to a better dispersion of ruthenium sulfide and therefore providing a higher amount of labile sulfur (CUS) according to $H_2$-TPSR patterns. Secondly, it strengths the Ru-S bond avoiding its reduction under the experimental condition as well as the sinterization of the active phase, preserving so the active sites.

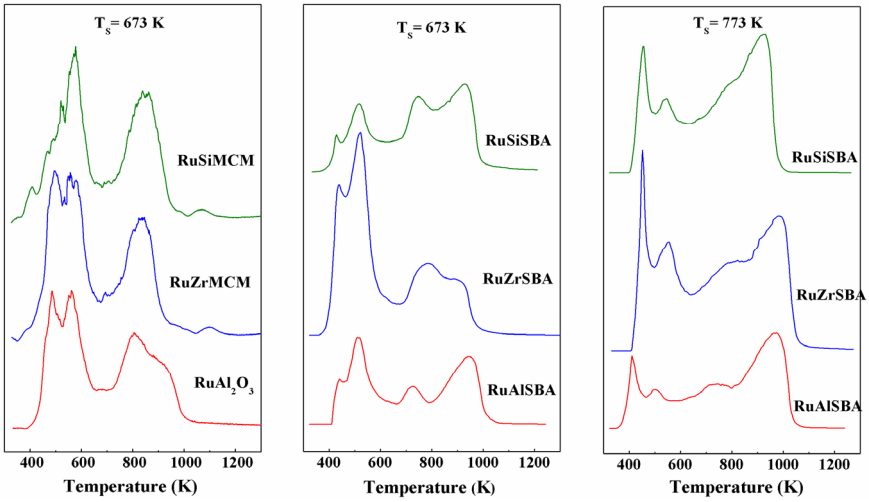


**Figure 5.** $H_2S$ desorption profiles for samples sulfided at 673 K (A and B) and samples sulfided at 773 K (C).

SBA-15 supported catalysts have also been sulfided at 773 K. By comparing the catalysts sulfided at 673 K and 773 K, in spite of presenting similar $H_2S$ bands, both the relative intensities and the peak maxima positions are different depending on the sulfidation temperature employed. In this sense, when sulfiding at 773 K the signals at $T < 573$ K decreases in intensity, while those at $T > 573$ K are more defined, what suggests that a higher amount of pyrite-type structure is formed, in accordance with previous works (De los Reyes et al., 1991) and also confirmed by XRD data. A similar profile at high temperatures has been reported by other authors (Castillo-Villalón et al., 2008), i.e., the asymmetry of this band, which can be decomposed into two contributions, is due to a surface reduction followed by bulk reduction. Castillo-Villalón et al. (Castillo-Villalón et al., 2008) have recently reported that in so far as the sulfidation temperature increases, the $H_2S$ evolving from species reduced at high temperature does, in detriment to some species that are reduced at low temperatures. Thus, by increasing the sulfidation temperature, some ruthenium sulfided species found when sulfiding at 673 K, are transformed into more stable

$RuS_2$ species when sulfiding at 773 K and that is why catalysts sulfided at 773 K present these bands more intense. Moreover, the peak maxima shift at higher temperatures, being this fact much more important in the bands at T > 573 K which are related to the reduction of $RuS_2$-pyrite phase. The formation of highly dispersed particles, as seen from TEM images, probably strongly interacting with the support, makes necessary a higher temperature to reduce them into the ruthenium metallic form (*vide infra*).

Regardless the material support employed, $H_2$-TPRS profiles of catalysts sulfided at 673 K do not present the bands at high temperatures with the characteristic reduction pattern of bulk $RuS_2$ in a pyrite-like structure. From these data, it can be concluded that at 673 K there is a great proportion of amorphous or poorly crystallize $RuS_2$ phase that is also less stable in HDS reactions. This fact should be much more important for catalysts supported on MCM type materials. XRD of spent catalysts reveals the formation of metallic ruthenium, while the diffraction bands of $RuS_2$ phase are not detectable. At 773 K, not only a greater formation of ruthenium sulfide in the form of pyrite but also the presence of amorphous ruthenium sulfide (intermediate temperatures) and sulfur excess on the surface (low temperature), are higher. The sample prepared on Al-SBA presents an increase in the $H_2S$ eliminated at higher temperatures, although this increment is less pronounced than for the other two samples.

Focusing on the catalysts sulfided at 773 K, which are much more active, TEM micrographs show the distribution of the active phase. Depending on the support employed, the location of $RuS_2$ is different. In general, no large ruthenium sulfur particles have been formed. The sulfided catalysts supported on Si-SBA and Zr-SBA show spherical particles with very small size, homogenously dispersed (Figure 6.A and 6.B) and mainly located inside the structure. The location of the ruthenium sulfide particles inside the pores of the mesoporous structure is clearly observed in Figure 6.A, where an alignment of the $RuS_2$ phase is observed. The distance between two rows corresponds to the $d_{100}$ parameter of the mesoporous structure. By measuring the distance between two rows, we obtain a value of 9.5 nm. If we compared this data with that calculated from the XRD pattern of the support at low angles, the $d_{100}$ reflection at $2\theta = 1.12^{o}$, we obtained an $a_0$ value of 9.1 nm. Therefore we can assess that ruthenium sulfide particles are homogeneously located inside the pores. On the other hand, the sulfided catalysts prepared from Al-SBA material support (Figures 6.C), present a different distribution of the active phase. We find small ruthenium sulfide particles inside the channels and larger particles located at the external surface of the support and scarcely interacting with it. A larger particle size is also found for these samples from XRD analysis.

From TEM analysis it can be seen that the small-sized particles are inside the pores of the carriers. Nonetheless the pores are not blocked by the incorporation of ruthenium, as long as, $N_2$ adsorption-desorption isotherms of sulfided catalysts are similar to the material support (isotherms of type IV), and only a slight decrease in the surface area is observed as a consequence of the location of $RuS_2$ particles inside the channels.

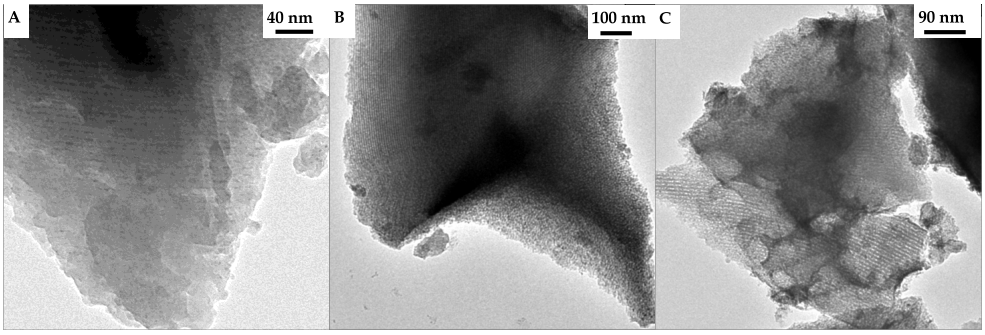


**Figure 6.** TEM micrographs for: A) RuSiSBA773, B) RuZrSBA773 and C) RuAlSBA773

The study of spent catalysts by TEM, reveals the great stability of $RuS_2$ particles during the test. While RuSiSBA and RuZrSBA present a homogenous distribution of small particles inside the pores, RuSiAlSBA shows a different distribution with zones presenting small and highly dispersed particles and mainly zones where agglomerates are present. Therefore, the better dispersion of the active phase is achieved when Si-SBA and Zr-SBA are used as supports.

As long as the catalytic performance of these systems is attributable to the formation of ruthenium sulfide, XPS spectra were recorded for sulfided and spent catalysts in order to elucidate the chemical state of the elements present. The Al 2*p*, O 1*s*, Si 2*p*, and Zr 3*d* core-level spectra were similar for sulfided and spent catalysts as well as their binding energies values maintained practically constant. Moreover, Table 6 lumps together the Ru $3p_{3/2}$ and S $2p_{3/2}$ binding energy values for all the samples, along with the S/Ru and Ru/X (X=Si+ (Si+Zr) or (Si+Al)) surface atomic ratios. Ruthenium species were analyzed by recording the Ru $3p_{3/2}$ spectrum of the samples and studied by an appropriate curve fitting. The signal is slightly asymmetric and can be decomposed into two contributions: the main one with its maximum between 460.8 and 461.4 eV; and a second one, much less intense whose maximum is between 463.2 and 463.8 eV. The main signal can be assigned to the $RuS_2$ phase. Mitchell et al. (Mitchell et al., 1987) reported, for ruthenium sulfide supported on alumina, Ru $3p_{3/2}$ binding energy values of 461.1-461-2 eV. On the other hand, the weak peak (463.2-463.8 eV) has been assigned to $RuCl_3$ species (Moulder et al., 1992). Catalysts supported on MCM-41 present Cl after the sulfidation procedure, therefore this band is due to $RuCl_3$. However, catalysts supported on SBA do not present the Cl 2*p* signal, and we suggest the presence of $Ru^{n+}$ species as responsible for such a band. The S $2p_{3/2}$ peak for sulfided catalysts is localized at BE ranged between 162.0 and 162.4 eV. This binding energy value is akin to that reported for sulfur forming disulfide polyanions $(S\text{-}S)^{2-}$ [8], i.e. sulfur forming $RuS_2$ with pyrite structure.

As far as spent catalysts are concerned, the Ru $3p_{3/2}$ signal hardly changes (data not shown), while the S 2*p* signal suffers a slight shift to lower binding energies and in some cases it is not detected. As reported for many authors (Berhault et al., 1997), during the catalytic run, due to the reducing atmosphere, sulfur can be eliminated from the catalyst surface and that

is why a modification of the S 2*p* signal is observed. In fact, from XRD analysis of spent catalysts, those sulfided at 673 K showed the presence of metallic ruthenium, confirming this fact. Moreover, Navarro et al. (Navarro et al., 1996) reported that a large amount of sulfur vacancies are generated when recording photoelectron spectra under a highly energetic X-ray beam impinging on the sample. This subject should also be kept in mind.

| Catalyst | Binding Energy (eV) | | | Surface atomic ratios | |
|---|---|---|---|---|---|
| | Ru 3*p* | | S 2*p*3/2 | | |
| | $RuS_2$ | $RuCl_3/Ru^{n+}$ | $S_2^{2-}$ | Ru/X* | S/Ru |
| **Ts=673K** | | | | | |
| **RuSiMCM** | 461.3 | 463.7 | 163.0 | 0.009 | 2.5 |
| **RuZrMCM** | 461.3 | 463.6 | 163.7 | 0.016 | 2.9 |
| **Ru-$Al_2O_3$** | 460.6 | 463.4 | 163.2 | 0.095 | 3.1 |
| **RuSiSBA** | 461.4 | 463.2 | 162.4 | 0.006 | 6.2 |
| **RuZrSBA** | 461.4 | 463.2 | 162.3 | 0.012 | 2.4 |
| **RuAlSBA** | 461.0 | 463.2 | 162.0 | 0.093 | 3.5 |
| **Ts=773K** | | | | | |
| **RuSiSBA** | 461.3 | 463.5 | 162.4 | 0.004 | 7.0 |
| **RuZrSBA** | 461.1 | 463.8 | 162.3 | 0.010 | 2.3 |
| **RuAlSBA** | 460.8 | 463.2 | 162.0 | 0.076 | 3.4 |

*X =Si, Si+Zr, Si+Al or Al, as accordingly

**Table 6.** Spectral parameters of $RuS_2$ supported catalysts.

Quantitative XPS data (Table 6) show that Ru/X atomic ratio for samples supported on Al-SBA and $Al_2O_3$ are what indicates a higher concentration of active phase on the surface, while the Ru/(Si+Zr) and Ru/Si surface atomic ratios have the lowest values. From TEM analysis, catalysts supported on Si-SBA and Zr-SBA present the majority of the active phase highly dispersed and mainly located inside the pores. Since SBA porous structure possesses a wall thickness of ca. 50 Å, these particles are not detected by XPS due to the surface sensitivity nature of this technique. The lower values for RuSiSBA and RuZrSBA corroborate what observed from TEM, i.e., the preferential location of the active phase inside the pores forming small particles. The S/Ru atomic ratios showed values higher than the stochiometric one due to the presence of an excess of sulfur on the surface, $H_2S$ or $SH^-$ groups formed during sulfiding process, which is not forming the pyrite phase. The analysis of spent catalysts showed a decrease in the S/Ru atomic ratio, in accordance with all the experimental exposed here and the literature reports, i.e., surface sulfur elimination occur during the catalytic test.

To sum up, the results reported here highlights the important role that the material support plays on the stability of the active phase, i.e., SBA type mesoporous materials provide ruthenium sulfide catalysts which are more active and stable in the HDS reaction of DBT than MCM-41 mesoporous one. Characterization results reveal that the bigger pore diameter of the former could lead to a better filling of them with the ruthenium sulfide. Moreover, after the

sulfidation processes the formation of $RuS_2$ with pyrite-type structure occurs in a greater extend on SBA-15 supported catalysts that is also more stable (XRD and $H_2$-TPSR), indicating a higher interaction of the precursor with SBA type material providing more stable $RuS_2$ particles, specially when the catalysts are sulfided at 773 K. The presence of heteroatoms depends on the type of mesoporous material employed, an increasing acidity is always observed, however no correlation is found between acidity and catalytic activity. While the incorporation of zirconium on MCM-41 seems to stabilise the $RuS_2$ phase and improving so the HDS behaviour; on SBA-15, no improvement is observed after heteroatoms addition, as long as Al doped support provides the least active catalysts; while Zr doped one (RuZrSBA) achieves the same level of activity than RuSiSBA only with the catalyst sulfided at 773 K. The presented data indicate that is the dispersion and distribution of the active phase what govern the catalytic behaviour of these systems and also the selectivity patterns. In this regard, the formation of small particles induces some preferential exposed planes, favouring the hydrogenation pathway as reported for other supported ruthenium sulfide catalysts (De los Reyes et al., 1991) what reveal the sensitivity to the structure of the $RuS_2$. Our results are in agreement with this statement, being RuAlSBA with the biggest particles sizes, the catalyst that provides the lowest values of selectivity to CHB, product formed in the hydrogenation route. Ishihara et al. (Ishihara et al., 1999) suggested that ruthenium atoms located on the surface and with anion vacancy are active in HDS. Thus, the bigger ruthenium sulfide crystals lead to a lower active surface and, as a consequence, to a lower activity.

The catalytic results reported here are similar to those reported for alumina supported ruthenium sulfide–cesium catalysts with metal loadings between 4 and 12 wt% (Ishihara et al.,1999). The strong interaction of $RuS_2$ particles with the pores leads to an equivalent performance to that obtained when alumina is doped with $Cs^+$ ions (Ishihara et al., 2004).

### 3.2. Influence of Cs as stabilizer agent of RuSiSBA catalyst

The addition of Cs to $RuS_2$ catalyst supported on Si-SBA-15 was studied in order to evaluate the role of Cs on the stabilization of $RuS_2$ phase, as reported in the literature. The influence of cesium content and sulfiding temperature (773 K and 873 K), as well as cesium precursor salt employed (cesium hydroxide and cesium chloride), was also studied. The quantity of ruthenium was maintained constant (7 wt%) while the amount of cesium variable, with Cs/Ru molar ratios of 0.1:1, 0.5:1, and 1:1. The catalysts will be denoted to as *x*Cs*y*Ru, being *x*:*y* the Cs/Ru molar ratio.

The catalytic results obtained for this family of catalysts in the HDS of DBT reaction is plotted in Figure 7, where $k_{HDS}$ values at a reaction temperature of 613 K are plotted for catalysts containing different amount of cesium and sulfided at 773 K and 873 K. For comparison, the catalytic data without cesium are also plotted (RuSiSBA). From this figure it can be clearly seen that the presence of cesium and the increment in the sulfidation temperature do not have a beneficial effect in terms of HDS activity, since the highest $k_{HDS}$ values is achieved for pure RuSiSBA sulfided at 773 K. It seems that the sulfiding process at higher temperature does not have enough influence on the catalytic activity.

With regards to selectivity values (Scheme 2), the results obtained here show that all catalysts follow the DBT HDS reaction through the DDS route, being even biphenyl the unique reaction product found for the catalysts with higher cesium loadings, being in line with the results reported by Ishihara (Ishihara et al., 1999). It follows the order 1Cs1Ru (100%)=0.5Cs1Ru (100%) > 0.1Cs1Ru (90.9%) > RuSiSBA (69.4%). Therefore, the hydrogenation capability decreases under the presence of Cs. Only the catalyst with a 0.1Cs:1Ru molar ratio presented a CHB selectivity of 10%.

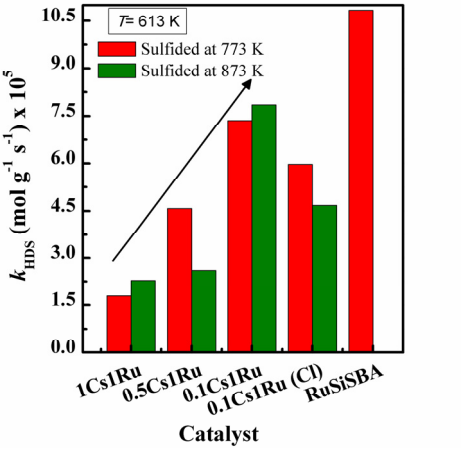


**Figure 7.** $k_{HDS}$ values as a function of cesium loading on the catalysts at a reaction temperature of 613 K

XRD results reveals that an agglomeration of the active phase occurs since the higher the cesium content the better defined the $RuS_2$ diffraction lines and therefore, the lower the dispersion. The same conclusion is extracted from textural properties, whose parameters decrease under the presence of cesium. It could be due to the formation $RuS_2$ agglomerates that provokes a blockage on the pores surface and hinders the access of nitrogen molecules. Moreover, the mean pore diameter also suffers a decrease but in a lesser extend. This is explained considering that agglomerates are blocking the entrance of some pores, however there are other ones where the metals are not deposited and are able to adsorb $N_2$ at 77 K, as can be clearly seen by TEM micrographs (*vide infra*).

Transmission electron microscopy elucidates the distribution of the active phase on the support. In general, it can be said that TEM analysis shows a heterogeneous distribution of the active phase, whose dispersion is totally dependent on cesium loading (Figure 8). The micrograph belonging to 1Cs1RuSTs catalyst is shown in Figure 8.A. At first glance, the micrographs show zones where there are big agglomerates on the external surface, assigned to the $RuS_2$ active phase according to EDAX analysis. Although there are some particles inside the pores, the dispersion of the active phase in the whole support is poor. Moreover, the analysis by EDAX in some zones of dispersed particles gave Cs/Cl atomic ratios close to 1 arising from the presence of CsCl compound. The sample with a Cs:Ru molar ratio of 0.5:1,

presents a micrograph (Figure 8.B) where the dispersion of the $RuS_2$ phase is better, although agglomerates are still present but in a lesser extend than before. The catalyst possesses an alignment of the particles, indicating that they are mainly located inside the pores of the support. However, when diminishing the cesium loading until a Cs:Ru ratio of 0.1:1, the dispersion of the active phase increases conspicuously, as can be clearly seen from Figure 8.C, where particles lower than 10 nm are highly dispersed an located inside the channels. The data presented here reveal that the lower the cesium content, the better the dispersion of the active phase.

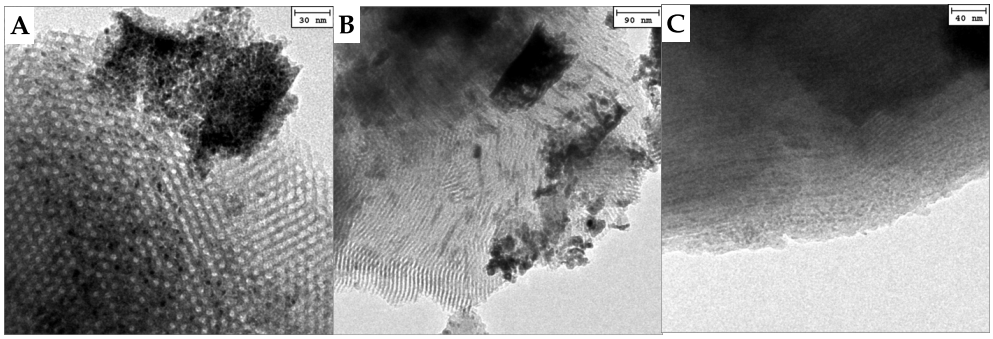


**Figure 8.** TEM micrograph for A) 1Cs1Ru catalyst, A) 0.5Cs1Ru catalyst and C) 0.1Cs1Ru catalysts sulfided at 773 K

In accordance with $H_2$-TPRS curves (Figure 9) the higher the cesium content the lesser the band intensities are. Moreover, the maxima of the curves are shifted to higher temperatures. In this regard, the 0.1Cs1Ru sample profile exhibits the most intense $H_2S$-release pattern that occurs at lower temperatures than that for 1Cs1Ru catalyst. It implies that the cesium content is the main reason of a low $H_2S$ elimination, i.e., a minor amount of labile sulfur is present on the catalysts.

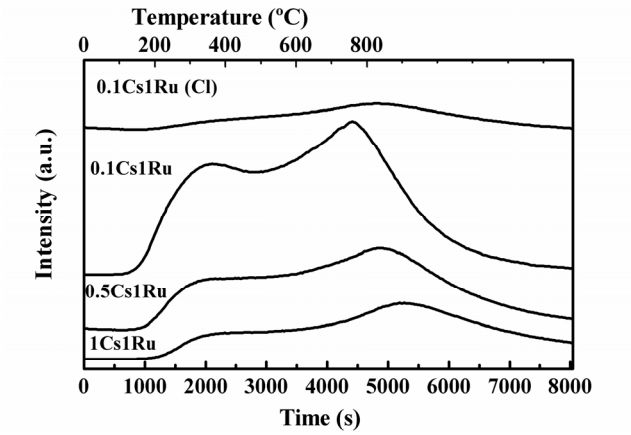


**Figure 9.** $H_2$-TPRS patterns of the catalysts sulfided at 773 K

The characterization and catalytic results indicate that the addition of cesium to a mesoporous material does not have a beneficial effect, mainly depending on the dispersion of the active phase attained. In this sense the higher the cesium content the lower the dispersion of the active phase and therefore the lower the catalytic activity in the DBT HDS reaction. Our results are contrary to those previously published in the literature. Ishihara, in a first work (Ishihara et al., 1996) studied the addition of alkali metal hydroxides to alumina-supported ruthenium catalysts and found that the cesium promoted catalyst was the most active. They reported that the location of cesium is close to ruthenium species, the dispersion of ruthenium species increases with an increase in the Cs/Ru ratio and furthermore the presence of cesium in close proximity to ruthenium atoms strengthens the bond of ruthenium and sulfur stabilizing ruthenium sulfide. In later works (Ishihara et al., 1998, 2003), they elucidated the behaviour of sulfur on the ruthenium catalysts and the role of cesium in HDS by radioisotope tracer methods, concluding that the mobility of sulfur on the catalysts decreased by the addition of cesium. On the contrary, the amount of labile sulfur on the catalyst increased with the amount of cesium added and reached the maximum at Ru:Cs=1:2 suggesting that Ru species in the catalyst was successfully dispersed on alumina. Further, it was reported that cesium promoted the C-S bond scission of DBT. With these premises and considering the characterization and activity results exposed here it can be pointed that the role of Cs to $RuS_2$ hydrotreating catalysts strongly depends on the support used. While the promoter effect of cesium on $\gamma$-$Al_2O_3$ is positive, on a mesoporous material such as SBA-15, the effect is negative. In this sense, the presence of cesium does not favour a good dispersion of the $RuS_2$ active phase, i.e., less cesium atoms are close to ruthenium atoms to stabilise the Ru-S bond and therefore the amount of labile sulfur also decreases by decreasing the dispersion. This is in agreement with our $H_2$-TPRS experiments that show an increase of the amount of $H_2S$ released with a decrease of cesium content in the catalysts, indicating that sulfur lability is inhibited in the presence of a large amount of Cs on the catalyst surface. The low dispersion of the active phase and the decreasing in the sulfur lability might explain the observed decrease in the catalytic activity with an increase Cs content in the catalysts (*vide supra*). Moreover, the presence of cesium altered the reaction mechanism in a way that only the product coming from the DDS route was obtained. By increasing the sulfiding temperature the catalytic activity did not improve considerably.

### 3.3. Influence of Cs precursor salt: CsOH versus CsCl

The catalyst with Cs:Ru molar ratio of 0.1:1 was also prepared from different cesium precursor salts, cesium hydroxide (0.1Cs1Ru) and cesium chloride (0.1Cs1Ru(Cl)), and sulfided at 773 K and 873 K. The catalytic results (Figure 7) showed that the catalyst prepared from cesium hydroxide exhibits a much higher HDS activity at both sulfided temperatures. The textural and structural properties of both catalysts are similar according to XRD, $S_{BET}$ and TEM analysis, i.e., they both present the same dispersion of the $RuS_2$ active phase. Notwithstanding the results extracted from TPRS results point to the different sulfur lability on both catalysts. The influence of the cesium precursor salt is more evident when the catalysts are sulfided at 773 K (Figure 7) where the differences found are very important, being the catalyst prepared from cesium hydroxide much more active.

The higher lability of sulfur in 0.1Cs1Ru sample was confirmed by DRIFT spectroscopy of adsorbed NO for both spent catalysts (Figures 10(a) and 10(b)). Thus, in Figure 10(a) the DRIFT spectra of NO adsorbed at room temperature onto both spent catalysts (after HDS at 613 K) are compared with that of NO adsorbed on pure SBA-15 support. As seen in this figure, both catalysts show two bands at 1905 and 1842 $cm^{-1}$ whereas the pure support shows one band centred at about 1860 $cm^{-1}$ and a shoulder at 1905 $cm^{-1}$. Additionally, all spectra show one band centred at 1875 $cm^{-1}$ due to NO adsorbed in its monomeric form in the gas phase (Dinerman et al., 1970). After subtraction of NO adsorbed on the pure support, the spectra of both spent catalysts show two bands at about 1900 and 1840 $cm^{-1}$ (Figure 10(b)) that could be tentatively ascribed to $(NO)_2$ dimmer species adsorbed on the Ru(Cs) sulfide phases. Interestingly, the spectrum of the most active catalyst in the HDS reaction at 613 K (0.1Cs1Ru) shows a band at about 1900 $cm^{-1}$ with a larger intensity than that of its counterpart prepared from cesium chloride, suggesting the presence of a larger amount of CUS sites. Moreover, TPO experiments revealed the higher amount of coke formed on 0.1Cs1Ru (Cl) catalyst, due to the presence of residual $Cl^-$ ions on the catalyst surface leads to an increase of the catalyst acidity which favours deactivation by coke formation.

The influence of the cesium precursor salt revealed that in spite of the same dispersion of the active phase, the usage of cesium hydroxide improved the amount of labile sulfur/the number of CUS sites and decreased the deactivation by coke.

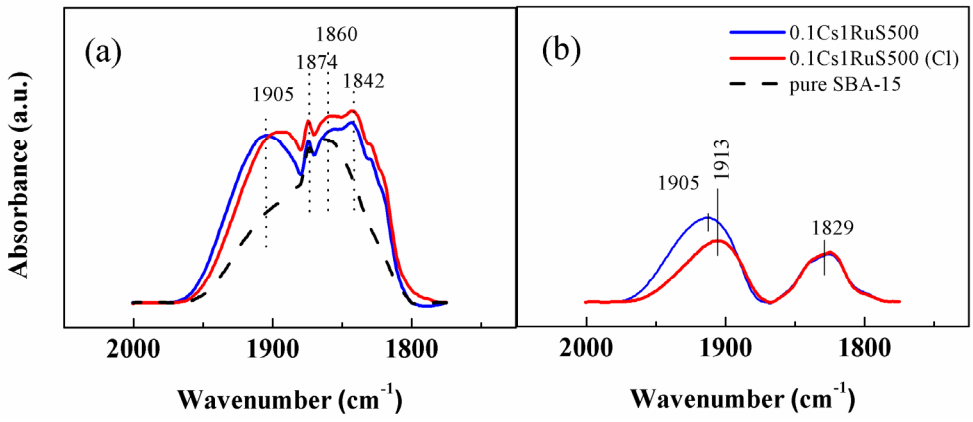


**Figure 10.** Influence of Cs precursor salt on the DRIFT spectra of NO adsorbed at room temperature for 10 min onto 0.1Cs1Ru (from CsOH) and 0.1Cs1Ru(Cl) (from CsCl) catalysts: (a) the spectra of spent catalysts (after HDS at 613 K) and pure SBA-15 support, (b) the difference spectra obtained after subtraction of NO adsorbed on pure support.

## Abbrevations

| | |
|---|---|
| DRIFT | Diffuse Reflectance Infrared Fourier Transform |
| EDAX | Energy Dispersive X-ray analysis |
| TEM | Transmission Electron Microscopy |
| TOS | Time On Stream |
| TPD | Temperature-Programmed Desorption |
| TPRS | Temperature-Programmed Reduction of Sulfur |
| WHSV | Weight Hourly Space Velocity |
| XPS | X-ray Photoelectron Spectroscopy |
| XRD | X-Ray Diffraction |

## Author details

A. Infantes-Molina
*Instituto de Catálisis y Petroleoquímica, CSIC, Cantoblanco, Madrid, Spain*

A. Romero-Pérez, J. Mérida-Robles, A. Jiménez-López and E. Rodríguez- Castellón*
*Dpto. de Química Inorgánica, Cristalografía y Mineralogía. Facultad de Ciencias, Universidad de Málaga, Campus de Teatinos, Málaga, Spain*

D. Eliche-Quesada
*Departamento de Ingeniería Química, Ambiental y de los Materiales, EPS de Linares, Universidad de Jaén, Jaén,Spain*

## Acknowledgement

We gratefully acknowledge the support from the Ministry of Science and Innovation, Spain (MICINN, España) through the project MAT2009-10481, the regional government (JA) through the Excellence projects (P07-FQM-5070) and FEDER funds. A.R.P thanks the CONACyT (México) for its financial support (Scholarship No. 189933). A.I.M. also thanks the MICINN, Spain, for a Juan de la Cierva contract.

## 4. References

Alstrup, I., Chorkemdorff, I., Candia, R., Clausen, B.S., & Topsøe, H. (1982). A combined XPS and Mössbauer emission spectroscopy study of the state of cobalt in sulfided, supported, and unsupported CoMo catalysts. *J. of Catalysis*, Vol. 77, No. 2, (October 1982), pp. (397-409). ISSN: 0021-9517.

Arteaga, A., Fierro, J.L.G., Delannay, F., & Delmon, B. (1986). Simulated deactivation and regeneration of an industrial CoMo/$\gamma$-$Al_2O_3$ HDS catalyst. *Applied Catalysis*, Vol. 26, (1986), pp. (227-249). ISSN: 0166-9834.

* Corresponding Author

Bataille, B., Lemberton, J.-L., Michaud, P., Perot, G., Vrinat, M., Lemaire, M., Schulz, E., Breysse, M., & Kasztelan, S. (2000). Alkyldibenzothiophenes HDS Promoter Effect, Reactivity, and Reaction Mechanism. *J. of. Catalysis*, Vol. 191, No. 2, (April 2000), pp. (409-422). ISSN: 0021-9517.

Benitez, A., Ramírez, J., Fierro, J.L.G., & López-Agudo, A. (1996). Effect of fluoride on the structure and activity of $NiW/Al_2O_3$ catalysts for HDS of thiophene and HDN of pyridine. *Applied Catalysis A: General*, Vol. 144, No. 1–2, (September 1996), pp. (343-364). ISSN: 0926-860X.

Berhault, G., Lacroix, M., Breysse, M., Maugé, F., Lavalley, J.C., & Qu, L. (1997). Characterization of Acid–Base Paired Sites on Silica-Supported $RuS_2$ by Infrared Spectroscopy and Methyl Mercaptan Condensation Reaction. *J. of Catalysis*, Vol. 170, No. 1, (August 1997), pp. (37-45). ISSN: 0021-9517.

Berhault, G., Lacroix, M., Breysse, M., Maugé, F., Lavalley, J.C., Nie, H., & Qu, L. (1998). Characterization of Acidic Sites of Silica-Supported Transition Metal Sulfides by Pyridine and 2,6 Dimethylpyridine Adsorption: Relation to Activity in $CH_3SH$ Condensation. *J. of Catalysis*, Vol. 178, No. 2, (September 1998), pp. (555-565). ISSN: 0021-9517.

Castillo-Villalón, P., Ramírez, J., & Maugé, F. (2008). Structure, stability and activity of $RuS_2$ supported on alumina. *J. of Catalysis*, Vol. 260, No. 1, (November 2008), pp. (65-74). ISSN: 0021-9517.

Corma, A., Martinez, A., Martinezsoria, V., & Monton, J.B. (1995). Hydrocracking of Vacuum Gasoil on the Novel Mesoporous MCM-41 Aluminosilicate Catalyst. *J. of Catalysis*, Vol. 153, No. 1, (April 1995), pp. (25-31). ISSN: 0021-9517.

De los Reyes, J.A., Göbölös, S., Vrinat, M., & Breysse, M. (1990). Preparation and characterization of highly active ruthenium sulphide supported catalysts. *Catalysis Letters,* Vol. 5, No. 1, (January 1990), pp (17–24). ISSN: 1572-879X.

De Los Reyes, J.A., Vrinat, M., Geantet, C., & Breysse, M. (1991). Ruthenium sulphide catalysts supported on alumina: physicochemical characterization and catalytic properties in hydrotreating reactions. *Catalysis Today*, Vol. 10, No. 4, (November 1991), pp. (645-664). ISSN: 0920-5861.

De Los Reyes, J.A. (2007). Ruthenium sulfide supported on alumina as hydrotreating catalyst. *Applied Catalysis A: General,* Vol. 322, (April 2007), pp. (106-112). ISSN: 0926-860X.

Dinerman, C. E., Ewing, G.E. (1970). IR Spectrum, Structure, and Heat of Formation of Gaseous $(NO)_2$ .*J. of Chemical Physics,* 1970, Vol. 53, No. 2, pp. (626–632). ISSN: 0021-9606.

Eijsbouts, S., van Gestel, J.N.M., van Oers, E.M., Prins, R., van Veen, J.A.R., & de Beer, V.H.J. (1994). In situ poisoning of the thiophene HDS activity of carbon-supported transition metal sulfide catalysts by phosphorus. *Applied Catalysis A: General*, Vol. 119, No. 2, (November 1994), pp. (293-303). ISSN: 0926-860X.

Eliche-Quesada, D., Mérida-Robles, J., Maireles-Torres, P., Rodríguez-Castellón, E., & Jiménez-López, A. (2003a). Hydrogenation and Ring Opening of Tetralin on Supported Ni Zr-Doped Mesoporous Silica Catalysts. Influence of the Ni Precursor. *Langmuir*, Vol. 19, No. 12, (May 2003), pp (4985–4991). ISSN: 0743-7463.

Eliche-Quesada, D., Mérida-Robles, J., Maireles-Torres, P., Rodriguez-Castellón, E., Busca, G., Finocchio, E., & Jiménez-López, A. (2003b). Effects of preparation method and sulfur poisoning on the hydrogenation and ring opening of tetralin on NiW/Zr-doped mesoporous silica catalysts. *J. of Catalysis*, Vol. 220, No. 2, (December 2003), pp. (457-467). ISSN: 0021-9517.

Eliche-Quesada, D., Mérida-Robles, J., Maireles-Torres, P., Rodriguez-Castellón, E., & Jiménez-López, A. (2004). Superficial characterization and hydroconversion of tetralin over NiW sulfide catalysts supported on Zr-doped mesoporous silica. *Applied Catalysis A: General*, Vol. 262, No. 1, (May 2004), pp. (111-120). ISSN: 0926-860X.

Eliche-Quesada, D., Mérida-Robles, J., Rodriguez-Castellón, E., & Jiménez-López, A. (2005). Ru, Os and Ru–Os supported on mesoporous silica doped with Zr as mild thio-tolerant catalysts in the hydrogenation and hydrogenolysis/hydrocracking of tetralin. *Applied Catalysis A: General*, Vol. 279, No. 1–2, (January 2005), pp (209-221). ISSN: 0926-860X.

Farag H., Mochida I., & Sakanishi K. (2000). Fundamental comparison studies on HDS of DBT over CoMo-based carbon and alumina catalysts. *Applied Catalysis A: General*, Vol. 194–195, (March 2000), pp. (147-157). ISSN:0926-860X.

Gil, A., Díaz, A., Gandía, L.M., & Montes, M. (1994). Influence of the preparation method and the nature of the support on the stability of nickel catalysts. *Applied Catalysis A: General*, Vol. 109, No. 2, (March 1994), pp. (167-179). ISSN: 0926-860X.

Gómez-Cazalilla, M., Mérida-Robles, J.M., Gurbani, A., Rodríguez-Castellón, E., & Jiménez-López, A. (2007). Characterization and acidic properties of Al-SBA-15 materials prepared by post-synthesis alumination of a low-cost ordered mesoporous silica. *J. of Solid State Chemistry*, Vol. 180, No. 3, (March 2007), pp (1130-1140). ISSN: 0022-4596.

Gómez-Cazalilla, M., Infantes-Molina, A., Mérida-Robles, J., Rodríguez-Castellón, E., & Jiménez-López, A. (2009a). Cr Species as Captors of S Molecules on Ni-Based Hydrotreating Catalysts. *Energy Fuels*, Vol. 23, No. 1, (February, 2009), pp. (101–110). ISSN: 0887-0624.

Gómez-Cazalilla, M., Infantes-Molina, A., Moreno-Tost, R., Maireles-Torres, P.J., Mérida-Robles, J., Rodríguez-Castellón, E., & Jiménez-López, A. (2009b). Al-SBA-15 as a support of catalysts based on chromium sulfide for sulfur removal. *Catalysis Today*, Vol. 143, No. 1–2, (May 2009), pp. (137-144). ISSN: 0920-5861.

Grzechowiak J.R., Mrozinska K., Masalka A., Góralski J., & Tylus W. (2006). Effect of MCM-41 on the physicochemical properties of Mo and NiMo catalysts and their performance in DBT conversion. *Catalysis Today*, Vol. 114, No. 2–3, (May 2006), pp. (272-280). ISSN: 0920-5861.

Hsu, C.S., & Robinson, P.R., (2006). *Practical Advances in Petroleum Processing*, Vol. 1, Springer. ISBN: 0-387-25811-6. New York.

Infantes-Molina, A., Mérida-Robles, J., Rodríguez-Castellón, E., Pawelec, B., Fierro, J.L.G., & Jiménez-López, A. (2005). Catalysts Based on Co/Zr-doped Mesoporous Silica MSU for the Hydrogenation and Hydrogenolysis/Hydrocracking of Tetralin. *Applied Catalysis A: General*, Vol. 286, No. 2, (June 2005), pp. (239-248). ISSN: 0926-860X.

Ishihara, A., Nomura, M., & Kabe, T. (1992). HDS of DBT Catalyzed by Alumina-Supported Ruthenium Carbonyl-Alkali Metal Hydroxide Systems. *Chemistry Letters.* Vol. 21, No. 12, (August 1992), pp. (2285–2288). ISSN: 1348-0715.

Ishihara, A., Nomura, M., Takahama, N., Hamaguchi, K., & Kabe, T. (1996). HDS of DBT Catalyzed by Supported Metal Carbonyl Complexes (Part5), Catalysts for HDS Prepared from Alumina-supported Ru Carbonyl-Alkali Metal Hydroxide Systems. *Sekiyu Gakkaishi*, Vol. 39, No. 3, (October 1996), pp. (211-221). ISSN: 0582-4664.

Ishihara, A., Yamaguchi, M., Godo, H., Qian, W., Godo, M., & Kabe, T. (1997). HDS of DBT Catalyzed by Supported Metal Carbonyl Complexes (Part 8), HDS of $^{35}$S-Labeled DBT on Alumina-Supported Ru Sulfide-Cesium Catalysts. *Sekiyu Gakkaishi,* Vol. 1, No. 1, (June 1997), pp. (51-58). ISSN: 0582-4664.

Ishihara, A., Godo, H., Kanamori, R., Qian, W., & Kabe, T. (1999). HDS of $^{35}$S-labeled DBT on Alumina–Supported Ruthenium Sulfide–Cesium Catalysts. *Applied Catalysis A: General*, Vol. 182, No. 2, (June 1999), pp. (345-355). ISSN: 0926-860X.

Ishihara, A., Lee, J., Dumeignil, F., Wang, A., Qian, E.W., & Kabe, T. (2003). Elucidation of Sulfidation State and HDS Mechanism on Ruthenium–Cesium Sulfide Catalysts using $^{35}$S Radioisotope Tracer Methods. *J. of Catalysis*, Vol. 217, No. 1, (July 2003), pp. (59-68). ISSN: 0021-9517.

Ishihara, A., Lee, J., Dumeignil, F., Yamaguchi, M., Hirao, S., Qian, E.W., & Kabe, T. (2004). Inhibiting Effect of $H_2S$ on the DBT HDS Activity of Ru-based Catalysts—Effect of the Cs Addition. *J. of Catalysis*, Vol. 224, No. 2, (June 2004), pp. (243-251). ISSN: 0021-9517.

Kloprogge, J.T., Welters, W.J.J., Booy, E., de Beer, V.H.J., van Santen, R.A., Geus, J.W., & Jansen J.B.H. (1993). Catalytic Activity of Nickel Sulfide Catalysts Supported on Al-pillared Montmorillonite for Thiophene HDS. *Applied Catalysis A: General*, Vol. 97, No. 1, (April 1993), pp. 77-85. ISSN: 0926-860X.

Kuo Y.J., Cocco, R.A., & Tatarchuk B.J. (1988). HYD and HDS over sulfided ruthenium catalysts: II. Impact of Surface Phase Behavior on Activity and Selectivity. *J. of Catalysis*, Vol. 112, No. 1, (July 1988), pp. (250-266). ISSN: 0021-9517.

Li, X., Wang, A., Wang, Y., Chen, Y., & Hu, Y. (2002). HDS of DBT over Ni–Mo Sulfides Supported by Protonexchanged Siliceous MCM-41. *Catalysis Letters,* Vol. 84, No. 1-2 (November 2002), pp. (107–113). ISSN: 1572-879X.

Li, X., Wang, A., Sun, Z., Li, C., Ren, J., Zhao, B., Wang, Y., Chen, Y., & Hu, Y. (2003). Effect of Surface Proton Exchange on HDS Performance of MCM-41-supported Catalysts.

*Applied Catalysis A: General*, Vol. 254, No. 2, (November 2003), pp. (319-326). ISSN: 0926-860X.

Liaw, S.J., Lin, R., Raje, A., & Davis, B.H. (1997). Hydrotreatment of coal-derived naphtha. Properties of zeolite-supported Ru sulfide catalysts. *Applied Catalysis A: General*, Vol. 151, No. 2, (April 1997), pp. (423-435). ISSN: 0926-860X.

Louwers, S.P.A., & Prins, R. (1992). Ni EXAFS Studies of the Ni-Mo-S Structure in Carbon-Supported and Alumina-Supported Ni-Mo Catalysts. *J. of Catalysis*, Vol. 133, No. 1, (January 1992), pp. (94-111). ISSN: 0021-9517.

Mangnus, P.J., Bos, A., & Moulijn, J. (1994). TPR of Oxidic and Sulfidic Alumina-Supported NiO, $WO_3$, and NiO-$WO_3$ Catalysts. *J. of Catalysis*, Vol. 146, No. 2, (April 1994), pp (437-448). ISSN: 0021-9517.

Mérida-Robles, J., Olivera-Pastor, P., Jiménez-López, A., & Rodríguez-Castellón E. (1996). Preparation and Properties of Fluorinated Alumina-Pillared $\alpha$-Zirconium Phosphate Materials. *The Journal of Physical Chemistry*. Vol. 100, No. 35, (August 1996), pp. (14726-14735). ISSN: 1932-7447.

Mitchell, P.C.H., Scott, C.E., Bonnelle, J.P., & Grimblot, J.G., (1987). Ru/Alumina and RuMo/Alumina Catalysts: An XPS study. *J. of Catalysis*, Vol. 107, No. 2, (October 1987), pp. ( 482-489). ISSN: 0021-9517.

Moulder, J.F., Stickle, W.F., Sobol, P.E., & Bomben, K.D. (October 1992). *Handbook of XPS*, Perkin-Elmer Corporation, ISBN:0-9627026-2-5. Minnesota, 1992.

Nava, R., Infantes-Molina, A., Castaño, P., Guil-López R., & Pawelec B. (2011). Inhibition of CoMo/HMS Catalyst Deactivation in the HDS of 4,6-DMDBT by Support Modification with Phosphate. *Fuel*, Vol. 90, No. 8, (August 2011), pp. (2726-2737). ISSN: 0016-2361.

Navarro, R., Pawelec, B., Fierro, J.L.G., & Vasudevan P.T. (1996). DBT HDS on Silica-Alumina-Supported Transition Metal Sulfide Catalysts. *Applied Catalysis A: General*, Vol. 148, No. 1, (December 1996), pp. (23-40). ISSN: 0926-860X.

Occelli, M.L., & Rennard, R.J. (1988). Hydrotreating Catalysts Containing Pillared Clays. *Catalysis Today*, Vol. 2, No. 2–3, (February 1988), pp.(309-319). ISSN: 0920-5861.

Okamoto, Y., Nakano, H., & Shimakawa, T. (1977). Stabilization effect of Co for Mo phase in Co-Mo/$Al_2O_3$ HDS catalysts studied with XPS. *J. of Catalysis*, Vol. 50, No. 3, (August 1977), pp. (447-454). ISNN: 0021-9517

Pawelec, B., Navarro, R.M., Campos-Martin, J.M., López-Agudo, A., Vasudevan, P.T., & Fierro, J.L.G. (2003). Silica–Alumina-Supported Transition Metal Sulfide Catalysts for Deep HDS. *Catalysis Today*, Vol. 86, No. 1–4, (November 2003), pp. (73-85). ISSN: 0920-5861.

Pecoraro, T.A., & Chianelli, R.R. (1981). HDS Catalysis by Transition Metal Sulfides. *J. of Catalysis*, Vol. 67, No. 2, (February 1981), pp. (430-445). ISSN: 0021-9517.

Quartararo, J., Mignard, S., & Kasztelan, S. (2000). HDS and Hydrogenation Activities of Alumina-Supported Transition Metal Sulfides. *J. of Catalysis*, Vol. 192, No. 2, (June 2000), pp (307-315). ISSN: 0021-9517.

Rodríguez-Castellón, E., Jiménez-López, A., Maireles-Torres, P., Jones, D.J., Rozière, J., Trombetta, M., Busca, G., Lenarda, M., & Storaro, L. (2003). Textural and Structural Properties and Surface Acidity Characterization of Mesoporous Silica-Zirconia Molecular Sieves. J. of Solid State Chemistry, Vol. 175, No. 2, (November 2003),pp. (159-169). ISSN: 0022-4596.

Ruette, F., & Ludeña, E.V. (1981). Molecular Orbital Calculations of the HDS of thiophene over a MoCo catalyst. J. of Catalysis, Vol. 67, No. 2, (February 1981), pp. (266-281). ISSN: 0021-9517.

Silva-Rodrigo, R., Calderón-Salas, C., Melo-Banda, J.A., Domínguez, J.M., & Vázquez-Rodríguez, A. (2004). Synthesis, characterization and comparison of catalytic properties of NiMo- and NiW/Ti-MCM-41 catalysts for HDS of thiophene and HVGO. *Catalysis Today*, Vol. 98, No. 1-2, (September 2004), pp. (123–129). ISSN: 0920-5861.

Song, C., & Reddy K.M. (1999). MCM-41 Supported Co–Mo Catalyst for HDS of DBT in Distillate Fuels. *Applied Catalysis A: General*, Vol. 176, No. 1, (January 1999), pp. (1-10). ISSN: 0926-860X.

Song, C., & Ma, X. (2003). New Design Approaches to Ultra-Clean Diesel Fuels by Deep Desulfurization and Deep Dearomatization. *Applied Catalysis B: Environmental*, Vol. 41, No. 1–2, (March 2003), pp. (207-238), ISSN: 0926-3373.

Topsoe, H., Clausen, B.S., Topsoe, N.-Y., Pedersen, E., Niemann, W., Müller, A., Bögge, H., & Lengeler, B. (1897). Faraday Transactions 1: Physical Chemistry in Condensed Phases. *J. of the Chemical Society,* Vol. 1, No. 83, (July 1987), pp. (2157-2167). ISSN:0300-9599.

Toulhoat, H., Raybaud, P., Kasztelan, S., Kresse, G., Hafner, J. (1999). Transition Metals to Sulfur Binding Energies Relationship to Catalytic Activities in HDS: Back to Sabatier with First Principle Calculations. *Catalysis Today*, Vol. 50, No. 3–4, (May 1999), pp. (629-636). ISSN: 0920-5861.

Vradman, L., Landau, M.V., Herskowitz, M., Ezersky, V., Talianker, M., Nikitenko, S., Koltypin, Y., & Gedanken, A. (2003). High Loading of Short $WS_2$ Slabs Inside SBA-15: Promotion with Ni and Performance in HDS and hydrogenation. *J. of Catalysis*, Vol. 213, No. 2, (January 2003), pp. (163-175). ISSN: 0021-9517.

Wang, A., Wang, Y., Kabe, T., Chen, Y., Ishihara, A., & Qian, W. (2002). HDS of DBT Over MCM-41-Supported Catalysts – II Sulfided Ni–Mo Catalysts. *J. of Catalysis*, Vol. 210, No. 2, (September 2002), pp. (319-327). ISSN: 0021-9517.

Welters, W.J.J., Vorbeck, G., Zandbergen, H.W., DeHaan, J.W., de Beer, V.H.J., & Van Sante, R.A. (1994). HDS Activity and Characterization of Zeolite-Supported Nickel Sulfide Catalysts. *J. of Catalysis*, Vol. 150, No. 1, (November 1994), pp. (155-169). ISSN: 0021-9517.

Whitehurst, D.D., Isoda, T., & Mochida, I. (1998). Present State of the Art and Future Challenges in the HDS of Polyaromatic Sulfur Compounds. *Advances in Catalysis*, Vol. 42, (1998), pp. (345-471). ISSN: 0-12-007844-9.

Yang, S. H., & Satterfield, C.N. (1983). Some Effects of Sulfiding of a $NiMoAl_2O_3$ Catalyst on its Activity for HDN of quinoline. *J. of Catalysis*, Vol. 81, No. 1, (May 1983), pp. (168-178). ISSN: 0021-9517.

Zepeda, T.A., Fierro, J.L.G., Pawelec, B., Nava, R., Klimova, T., Fuentes, G.A., & Halachev, T. (2005). Synthesis and Characterization of Ti-HMS and CoMo/Ti-HMS Oxide Materials with Varying Ti Content. *Chemistry of Materials.* Vol. 17, No. 16, (May 2005), pp. (4062–4073). ISSN: 0897-4756.